Establishing Aluminum-Oxygen (Al-O) Equilibria in Liquid Iron at 1873 K: An Experimental Study and Thermodynamic Analysis

MIR ISHFAQ and MANISH M. PANDE

Aluminum-oxygen equilibria for varying concentration of aluminum (0.0008–23.35 wt pct) content have been established at 1873 K. The experiments were carried out in an inert (high-purity argon) atmosphere by melting pure electrolytic iron with master alloy of Fe-Al in an alumina crucible and equilibrating the Fe-Al-O melt at 1873 K for two hours. A two-stage heating method in an inert gas fusion absorptiometry and scanning electron microscopy-automated inclusion analysis (SEM-AIA) have been employed to estimate the insoluble oxygen content in the samples. Aluminum-oxygen equilibria have been established separately for the total and dissolved oxygen contents. Thermodynamic analysis has been carried out using higher order interaction parameters, namely, Wagner interaction parameter formalism (WIPF) truncated at 2nd order, Darken's quadratic formalism, and the Cubic formalism. Among these formalisms, the experimental analysis has been found to be in good agreement with thermodynamic analysis based on Cubic formalism.

I. INTRODUCTION

THE recent developments in advanced high strength steels (AHSS) such as twinning induced plasticity (TWIP) and transformation induced plasticity (TRIP) steels have an exquisite effect in the future automobiles due to their excellent combination of formability, ductility, and strength. In these steel grades, the role of aluminum is not limited to deoxidizer, but it is also added as an alloying element. Therefore, it is critical to examine and investigate Al-O equilibria in such steels in the high Al concentration range. Al-O equilibria in the low aluminum concentration range have been well established by several researchers which are in good agreement with each other.[1–16] However, in the high aluminum concentration range, a large discrepancy has been reported between the experimental data of different researchers. As pointed out by Zhang et al.,[16] one of the prime reasons could be the overestimation of oxygen because of alumina inclusions. Larger alumina particles usually float if a sufficient time is given at the

equilibration temperature for flotation. However, some of the particles, depending on the location, can still be present in the melt during the sampling. Subsequently, these (primary) alumina particles, in addition to the secondary alumina particles precipitated during cooling/solidification, contribute to the total oxygen (TO) content of the steel samples. The driving force for the formation of secondary inclusions is the increase in supersaturation as the temperature decreases during cooling/solidification. Several experiments were done to separate the alumina particles efficiently from the steel melt. Suito et al.[9] performed Al-O deoxidation experiments using alumina and CaO crucibles, with and without use of CaO-Al$_2$O$_3$ as top slag. When slag is utilized, it becomes apparent that a majority of the initial (primary) inclusions have risen to the surface. The aluminum that is insoluble in acid will be obviously linked to alumina inclusions. Therefore, acid-insoluble aluminum was associated with secondary inclusions. This was reinforced by the observation that acid-insoluble aluminum remained relatively unaffected by the overall aluminum concentration. In this scenario, the total aluminum and total oxygen levels at 1873 K could be aligned with dissolved aluminum and dissolved oxygen. They also attempted to separate secondary inclusions by re-heating the solidified ingot to 1873 K so that these (secondary) inclusions would be absorbed by the top calcium aluminate slag layer. In the present work, dissolved or soluble oxygen O has been distinguished from the insoluble oxygen (oxygen present in the form of inclusions) to establish the true Al-O

MIR ISHFAQ and MANISH M. PANDE are with the Department of Metallurgical Engineering and Materials Science, Indian Institute of Technology Bombay, Mumbai, Maharashtra 400076, India. Contact e-mail: manish.pande@iitb.ac.in

equilibria. Rhode et al.[6] also used CaO-Al$_2$O$_3$ flux on the top of liquid steel for the removal/separation of alumina inclusions from the melt. They assumed that the activity of alumina as one considering the saturation of CaO-Al$_2$O$_3$ flux with alumina. The Japan Society for the promotion of Science (JSPS)[17] recommended the values reported by Rhode et al.[6] as it was the most reliable data at that time. Recently, Zhang et al.[16] also adopted the same methodology to minimize the presence of alumina particles/inclusions in the melt. Interestingly, all the three researchers (Rhode et al.,[6] Suito et al.,[9] and Zhang et al.[16]) reported high total oxygen content than Kang et al.[13], Paek et al.[14] and the results obtained in the present study, in the aluminum concentration range of 1–5 wt pct. In our current study, we obtained as low as 2 ppm of dissolved oxygen (and 3.333 ppm of total oxygen) and the same result was obtained by Kang et al.[13] and Paek et al.[14] Paek et al. used CaO-Al$_2$O$_3$ flux, beyond the aluminum concentration of 33 wt pct. However, such practice (addition of flux on the top of steel melt) can lead to the ingression of exogenous inclusions. Slag also has the potential to react with the crucible wall thus transferring more inclusions to the melt. Surface contamination and suspended oxide particles also lead to the overestimation of oxygen.[10]

Another source of error in oxygen concentration was identified by Yin et al.[18] The continuous removal of dissolved oxygen ($\underline{O}$) by the addition of aluminum makes it oxygen deficient. So, at a high concentration of aluminum, there will not be enough dissolved oxygen that can take part in the deoxidation equilibrium. To counter this problem, Paek et al.[14] added Fe$_2$O$_3$ powder into the Fe-Al alloy melt. A proper reasoning and trend were missing in the reported data (for Fe$_2$O$_3$) addition as Paek et al.[14] obtained oxygen as low as 1.8 ppm and 2.8 ppm at Al concentration of 9.06 and 1.64 pct, respectively, while it was maximum (9.8 ppm) at an Al concentration of 8.04 pct. The plausible source of discrepancy can also arise while measuring oxygen using inert gas infrared spectroscopy. The vaporized aluminum can react with CO and form Al$_2$O vapor which condenses at low temperature thus underestimating the actual oxygen content. This phenomenon is called gettering effect and results in aberration of precision in oxygen measurement. Several authors[9,11–13] have used Sn bath-Ni capsule coupled with graphite crucibles to counter this problem. This usually occurs at high aluminum concentration.

Much of the disagreement among the values of the oxygen content reported by several researchers is also because of the different experimental and characterization techniques employed to establish Al-O equilibria. The summary of the previous experimental studies is provided in Table I. Over the years, sophisticated instruments have brought much reliability in obtaining the experimental data. Hilty and Crafts[1] obtained oxygen content in the range of 1500 to 15 ppm which is quite unusual from the viewpoint of modern researchers. This can be well comprehended in the experimental results of Paek et al.[14] where they obtained oxygen as low as 1.8 ppm and maximum as 84.6 ppm. Over the past two decades, inert gas fusion infrared

absorptiometry has replaced vacuum fusion analysis and neutron activation method for total oxygen measurement. Recently, Kang et al.[19,20] have introduced a two-stage heating method to distinguish the dissolved oxygen from the total oxygen using an inert gas fusion infrared absorptiometry. The dissolved oxygen present in the steel sample reacts with carbon when the sample is molten around 1873 K. At a temperature of more than 2073 K, the alumina is completely reduced by carbon forming CO thus providing an estimate about the insoluble oxygen, that is, the combined oxygen or oxygen present in the form of oxide particles. In a normal analysis, the steel sample is heated rapidly in a single stage to a very high temperature to release analyte gases. Sampling technique remains one of the prime influencing factors. It is crucial to draw and cool the samples in a controlled atmosphere to avoid the contamination. The possibility of reoxidation increases during the sampling and quenching.

In the present study, we have devised a novel methodology to obtain the steel samples for the compositional analysis. All the experiments were carried out in a resistance heated furnace in an inert atmosphere using a small quantity of steel (90–100 g). Care was taken to maintain an inert atmosphere throughout the experiments, that is, from room temperature to 1873 K, and cooling from 1873 K to room temperature. In the present work, we overcome the limitations usually encountered during the high temperature experiments, for instance, (i) maintaining a constant temperature zone of 1873 K by using a resistance heated furnace, (ii) contamination of the furnace (inert) atmosphere and the steel melt was altogether avoided as no additions and the sampling were done during the experiment, and (iii) starting oxygen content was nearly constant (100–120 ppm) for all the experiments as an individual experiment was carried out for each Al concentration. Thus, the deficiency of oxygen was not a constraint in the present experiments. After melting and equilibrating the melt for two hours, cooling was done in the furnace itself with a continuous supply of deoxidized argon. The individual samples were carefully cut-off from the central bottom portion of solidified ingot to carry out elemental and inclusion analysis. The detailed sampling methodology is given in the next section.

Solidification of the steel samples in the present work was somewhat different (or slower) from the quenching methods used by other researchers. Quenching at 1873 K gives more or less an illustration of an equilibrium at the particular temperature. However, such practice requires the sampling to be done using (a) an additional sampler (possibility of contamination) and/or disturbance in the furnace atmosphere (chance of air ingression and reoxidation) and (b) the sampling location may vary in the steel melt containing the alumina particles in a state of flotation. Moreover, such practice has little relevance in the industrial scale where the complete solidification time for steel melt may take several minutes to hours depending on the ingot size. The center of ingot takes some time to cool down and the reactions would start occurring at some lower temperature. Thus, the actual equilibrium (established at

Table I. Summary of Experimental Techniques Carried out by Different Researchers

Researchers	Experimental Method (Furnace Atmosphere and Oxygen Analysis Technique)	Pct Al range	Temperature range	Year	References
Hilty and Crafts	Rotating Crucible Induction furnace/Argon/Vacuum fusion analysis	0.0001 to 1	1823–1923 K	1950	1
Gokcen and Chipman	H_2-H_2O/Induction heating/Vacuum fusion analysis	0.0038 to 0.057	1968–2139 K	1953	2
Mclean and Bell	H_2-H_2O/Vacuum fusion analysis	0.003 to 0.067	1996–2096 K	1965	3
Swisher	Fe (l)-Al_2O_3(s)/Vacuum fusion analysis	0.009 to 12	1853 K	1967	4
Fruehan	Vertical Mo wire wound resistance furnace, Purified argon, EMF, and Neutron activation method	0.02 to 1.4	1873 K	1970	5
Rhode et al.	Tanmann furnace, Argon, Fe(l)-CaO-Al_2O_3 slag	0.01 to 2.5	1873–2023 K	1971	6
Janke and Fischer	EMF	0.0003 to 1.3	1873 K	1976	7
Shevtsov	Fe(l)-Al_2O_3(s)/Vacuum fusion analysis	0.01 to 100	1873 K	1981	8
Suito et al.	LaCrO3 resistance furnace, Deoxidized argon, Fe(l)-CaO-Al_2O_3(s)/Inert gas fusion infrared absorptiometry	0.0011 to 32.7	1873 K	1991	9
Dimitrov et al.	Tanmann furnace, Fe(l)-Al_2O_3(s), EMF	0.0001 to 1.2	1873 K	1995	10
Seo et al.	LaCrO$_3$ resistance furnace, Deoxidized argon, Fe(l)- Al_2O_3(s)/Inert gas infrared absorptiometry	0.0002 to 0.9873	1873 K	1998	11
Hayashi et al.	Induction furnace, Purified argon, Fe(l)-Al_2O_3/Inert gas fusion infrared absorptiometry	0.00031 to 0.0495	1873 K	2008	12
Kang et al.	Tanmann furnace, Argon + 3 pctH$_2$, Fe(l)- Al_2O_3(s)/Inert gas infrared absorptiometry	0.014 to 9.046	1873 K	2009	13
Paek et al.	Induction furnace, Deoxidized argon, Fe(l)-Al_2O_3(s), Fe(l)-CaO-Al_2O_3 slag /Inert gas infrared absorptiometry	0.0027 to 100	1873–1923 K	2015	14
Fukaya et al.	Vertical resistance furnace/Argon	0.00024-0.1108	1773–1873 K	2018	15
Zhang et al.	Resistance heating furnace/Ar-H$_2$/, Fe(l)-CaO-Al_2O_3-CaF$_2$ flux/Inert gas fusion infrared absorption spectroscopy	0.019 to 14.51	1873 K	2022	16
Present work	Vertical tube furnace (MoSi2 resistance)/deoxidized argon/Fe(l)- Al_2O_3(s)/Inert gas infrared absorptiometry, SEM-AIA.	0.0008 to 23.35	1873 K	2023	Present study

steelmaking temperature which is typically 1873 K) gets disturbed due to the secondary precipitation of oxide particles in the melt.[15] Though our actual intention was not to simulate the industrial practice of aluminum addition in a high concentration range, some of the present results may be correlated to the industrial practice of aluminum alloying. This has also been discussed in the subsequent sections. The contribution of secondary alumina particles formed during furnace cooling (along with the suspended alumina particles formed due to the primary deoxidation) have also been considered by quantifying the combined oxygen using two techniques (1) Scanning Electron Microscopy–Automated Inclusion Analysis (SEM-AIA) for selected samples and (2) two-stage heating method in an inert gas fusion infrared absorptiometry. It should be noted here that the dissolved oxygen at 1873 K can be approximated as total oxygen measured in the solidified samples for two reasons, (i) the equilibration time (2 hours at 1873 K) for the experiments was relatively high and sufficient for the flotation of large-sized inclusions formed due to primary deoxidation (ii) the solidification time for the samples was around 15–20 minutes which is insufficient for the separation/flotation of micron sized particles (formed due to secondary precipitation) from the central bottom portion of the solidified ingot which was the sampling location in our work. Therefore, the dissolved oxygen may change, however, the total oxygen (after solidification) which constitutes the dissolved and the combined oxygen should be approximately the same as dissolved oxygen at equilibration temperature (1873 K). Nevertheless, the other possibilities pertaining to the presence of inclusions have been elaborately covered in the 'Discussion' section. The present experiments were quite close in establishing the true Al-O equilibria at 1873 K overcoming most of the limitations of the previous studies.

The experimental study has also been supplemented with the thermodynamic analysis. Three different formalisms have been employed to assess the thermodynamic equilibrium between aluminum and oxygen, namely, Wagner's Interaction Parameter Formalism (WIPF)[21] truncated at the 2nd order (also known as Lupis Elliott's formalism), Darken's quadratic formalism[22] analogous to WIPF truncated at the 2nd order with thermodynamic consistency, and the Cubic formalism analogous to WIPF (truncated at the 3rd order with thermodynamic consistency).[23] The essence for employing the higher order formalism has been explained in the "Discussion" section. Usually, the first-order truncated series is widely used by steelmakers owing to its mathematical simplicity and requirement of less interaction parameters. However, its main disadvantage is that it restricts its application at finite concentrations. WIPF truncated at the 1st order was made thermodynamically consistent by Pelton et al.[24] by incorporating the $\ln\gamma_{solvent}$ term in the Taylor's series expansion of $\ln\gamma_{solute}$. Srikanth and Jacob[25] endeavored to obtain expression of $\ln\gamma_{solvent}$ using path integration. Pelton[26] questioned this approach and pointed out that these expressions did not obey the Maxwell's relationship regardless of the expression of $\ln\gamma_{solvent}$. As

mentioned by Malakhov,[27] imposing such constraint renders the interaction parameter formalism ineffective (as all the interaction parameters becomes equal) when dealing with finite concentrations. Malakhov introduced a corrective function $\phi(x_2, x_3)$ in the expressions of activity coefficient of solute ($\ln\gamma_{solute}$) to make it thermodynamically consistent. Further, he mentioned that there are limitless ways of corrections in WIPF to make it thermodynamically consistent. Kang[28] mentioned that this corrective function can be obtained uniquely by integrating the 1st order differential of $\ln\gamma_{solute}$ and also by differentiating the 2nd order polynomial representing excess molar Gibbs free energy. This preserves thermodynamic consistency. In the present work, Wagner's 2nd order formalism has been treated without thermodynamic consistency, while both Quadratic and Cubic formalism satisfy conditions of thermodynamic consistency namely, Gibbs-Duhem equation and Maxwell's relationship. This has been shown in our previous work.[23]

In our present work, we have estimated the values of the (cross, ternary) interaction parameters ($\varepsilon_j^i, \rho_k^{i,j}, \theta_l^{i,j,k}$), dimensionless coefficients ($\omega_k^{i,j}, \omega^{i,j,k}$) , and the equilibrium constants (K) based on the three formalisms using the present experimental data.

Redlich-Kister (R-K) polynomial of the 3rd order has been previously used by Fukaya et al.[15] and Zhang et al.[16] The R-K polynomial represents the excess molar free energy (g^E) of the system. However, one of dimensionless coefficients $\omega^{Fe,Al,O}$ which was missing in the polynomial expression of g^E for Fe-Al-O ternary system has been incorporated in the present study. Using the experimental data obtained in the present study, we have calculated its value which is insignificant compared to most of other coefficients. However, the coefficient cannot be ignored for the sake of correctness. Another important aspect is compilation of interaction parameter data based on all the three formalisms (WIPF, Darken, and Cubic formalism) which was missing in the previous literature. The relationship between (i) aluminum and total oxygen (TO) as well as (i) aluminum and dissolved oxygen (O) has been obtained on a weight percent scale using these formalisms. The explanation for establishing Al-O equilibria separately for O or TO (measured in the solid samples) has been extensively discussed in 'Section "IV.A" Experimental analysis.'

II. EXPERIMENTAL

A. *High Temperature Melting Experiments*

A vertical tube furnace (Carbolite GERO) with heating element $MoSi_2$ was used for establishing the deoxidation equilibria at 1873 K. The temperature and heating rate were controlled by a nano dac controller and the accuracy was determined within ±2 K. B type thermocouple (Pt-Pt/Rh) was used to locate the exact temperature zone of 1873 K inside the tube. A uniform temperature zone of about 6 cm length inside the tube

(57–63 cm from the top) was determined. Small electrolytic iron chunks (weighing around 60–90 grams) along with Fe-Al master alloy were kept in the pure alumina crucible (99.99 pct pure) and the crucible was kept in the uniform temperature zone where the variation was within ±2 K. Before heating, the furnace was flushed with deoxidized argon at a flow rate of 7 liters/h for 6 hours to remove the residual gases from the furnace tube. The furnace was then switched on and the heating rate was kept at 5 K/minute. Argon (99.99 pct) was passed first through silica gel and molecular sieves to remove the moisture. It was then passed through a bed of copper turnings kept in a silica tube heated to the temperature of 673 K. The partially deoxidized argon gas was then passed through stainless steel tube heated to the temperature of 773 K stuffed with magnesium shavings loosely. The main aim of passing argon gas through heated copper turnings and magnesium shavings was to decrease the partial pressure of oxygen in argon gas so as not to oxidize the iron kept in the crucible. This was verified by melting pure iron in the furnace at 1873 K. The total oxygen measured in the solidified samples (without any addition) was constant and was in the range of 100–120 ppm (0.01–0.012 wt pct). At 1873 K, the sample was kept for two hours to provide sufficient time for equilibrium and flotation of alumina particles from the melt. The crucible was cooled in the furnace and the deoxidized gas was passed continuously till the sample was brought to room temperature. A total of 24 experiments were carried out and each solidified ingot was considered as one experiment (Figure 1).

B. Characterization of samples

1. Compositional analysis

The detailed sampling methodology for obtaining compositional and inclusion analysis is shown in Figure 2. The samples for the analysis were cut-off from a sliced section (thickness 10 mm), about 5 mm above the bottom portion as most of the alumina inclusions floated toward the surface owing to the low density. However, some inclusions (with extremely small size) might be present near the bottom region. The small chips/cuboidal samples for aluminum and oxygen analysis were taken from this central bottom (CB) region with the use of wire electrical discharge machine (EDM) (BAOMA, BMW-3000 DK7725). A small chip of thickness 0.7 mm and weight of 0.1 g was taken out and its surface was polished using emery paper to remove the oxidized layer. It was then ultrasonically cleaned in acetone (99.99 pct grade) for at least 30 minutes. The sample was then dissolved in aqua regia (70 pct HCl and 30 pct HNO_3). The solution was then analyzed for quantitative determination of aluminum content using Inductively Coupled Plasma -Atomic Emission spectroscopy (ICP-AES, SPECTRO ARCOS). For oxygen measurement, a cuboidal sample of (4mm×5mm×8mm) with an approximate weight of 0.7–1 g was taken and its surface was polished with emery papers (from P100 to P2500) followed by diamond polishing to ensure removal of any surface

contamination. Surface cleaning of samples is necessary as iron oxide layer on the top of steel sample can contribute up to 0.0002 wt pct (2 ppm) of oxygen.[29] The samples were then ultrasonically cleaned using acetone to ensure removal of any adhered impurities. These samples were stored in the acetone in a closed plastic bottle, and taken out and dried only at the time of oxygen analysis. The oxygen content in the samples was measured using inert gas fusion infrared absorptiometry (LECO, ON736). The equipment was calibrated for an oxygen content using standard steel pin (Lot 0634, Part No. 502-928) containing 0.0036 ± 0.0004 wt pct oxygen. For oxygen analysis, the average of two samples cut from the central bottom region of the solidified ingot was taken for each experiment. Each sample was analyzed with a novel two-stage heating method to differentiate dissolved oxygen from the insoluble one. The two-stage heating method developed by Kang et al.[19,20] is an innovative technique to distinguish dissolved (soluble) oxygen and combined (insoluble) oxygen in steels. The method exploits the different reaction temperatures required to release dissolved oxygen (through C-$\underline{O}$ reaction) and the combined oxygen present in the form of alumina particles (through C-Al_2O_3 reaction). The sample was first heated to a temperature of 1873 K in a graphite crucible to ensure that the dissolved oxygen from the (molten) steel sample reacts with C from the (graphite) crucible. This corresponds to the release of dissolved oxygen from the melt as given in Eq. [1]

$$C_{(graphite)}\underline{O} = CO(g) \qquad [1]$$
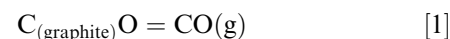
In the second stage, the same sample was further heated to 2613 K. At this temperature, the carbothermic reduction of alumina inclusions would happen and a new peak corresponding to the oxygen combined with alumina inclusions, that is insoluble (IO) would appear.

$$Al_2O_{3(solid)} + C_{(graphite)} = 3CO_{(g)} + 2\underline{Al} \qquad [2]$$
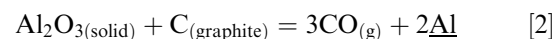
Typically, in a single-stage heating (2613 K), the peak corresponds to the total oxygen providing an estimate of dissolved and insoluble (combined) oxygen together, that is, the total oxygen.

2. Inclusions analysis

Selected samples (containing varying aluminum concentration) were analyzed using scanning electron microscopy (SEM) analysis (Zeiss 45-58 Auriga Compact) to investigate the characteristics of non-metallic (alumina) inclusions/particles. The alumina particles were identified in the samples with Energy Dispersive Spectrum (EDS) and the elemental mapping simultaneously. Scanning Electron Microscopy Automated Inclusion analysis (SEM-AIA) has also been carried out to investigate the characteristics of several hundred alumina particles in the selected samples (with cross sectional area of 8 mm × 12 mm). The insoluble oxygen measured using two-stage heating method (LECO) has been correlated with the insoluble oxygen obtained/derived from the statistically significant number of alumina inclusions analyzed with SEM-AIA. The total
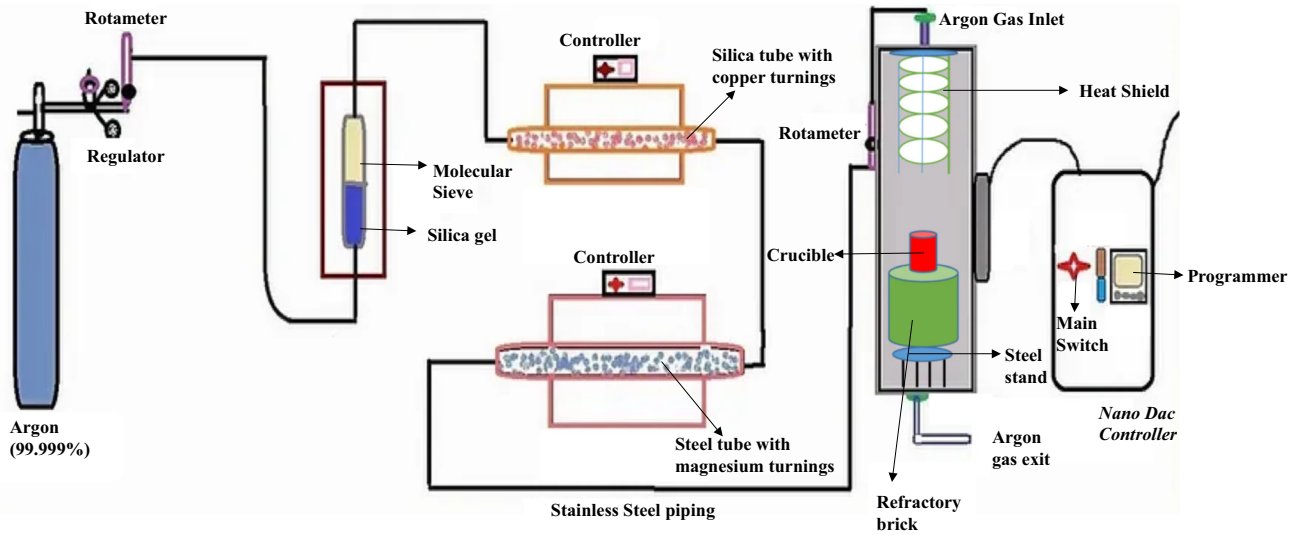
Fig. 1—Schematic of the high temperature experimental set up.
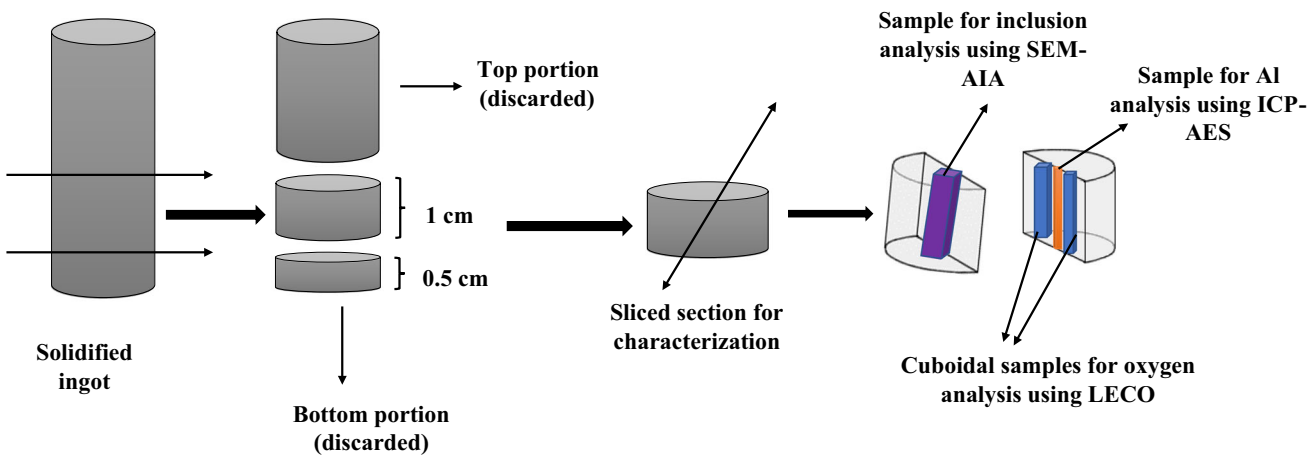

Fig. 2—Various samples obtained from solidified ingot for compositional and inclusion analysis.

oxygen content in the steel samples, in the low Al concentration range, has been found to be very small. In the present as well as in the previous studies,[1–16] it has been observed that as the aluminum content in the steel increases beyond a certain critical value, the equilibrium oxygen content also increases. The tendency to retain more oxygen with increase in aluminum content has not been satisfactorily explained using various thermodynamic formalisms/models. Therefore, it was important to obtain the combined/insoluble oxygen in the high Al concentration range. The selected samples in a high Al concentration range were chosen for SEM-AIA analysis since the primary objective of this investigation was to determine the oxygen present in the form of alumina inclusions. The area fraction of several hundred alumina particles was measured using SEM-AIA, (Bruker Esprit Steel). The working distance was set as 10 mm and the analyzed particle size range was set between 549 nm (4 pixels) and 30 μm.

Assuming that the alumina particles were distributed homogenously, the area fraction can be taken as the volume fraction of particles.[30] This is a reasonable assumption since the SEM-AIA was carried out on the sample taken from the central bottom (CB) region of the solidified ingot. In this CB region, homogenous distribution of the alumina inclusions can be expected.

Total oxygen in the sample (TO)= Dissolved oxygen in steel (O) + insoluble oxygen present as alumina inclusions (IO) + O content in the oxide film (O_F)

The third term (O_F) in the above expression for total oxygen can be neglected since the samples were stored in the acetone from the time of cutting them off from solidified ingot until its absorptiometry analysis and the oxygen content in the oxide film is usually very small.[29]

Therefore, the actual expression for the total oxygen content can be given as

$$TO = \underline{O} + IO \qquad [3]$$

The expression for the percentage of insoluble oxygen can be approximated by the following formula.[30]

$$\text{IO}(wt\ pct) = \frac{\rho_{\text{Al}_2\text{O}_3} \times \Sigma s_A(I)}{\rho_{\text{Fe-Al}}[\Sigma s_A(T) - \Sigma s_A(I)] + [\rho_{\text{Al}_2\text{O}_3} \Sigma s_A(I)]} \times \frac{3M_O}{M_{\text{Al}_2\text{O}_3}} \times 100,$$

[4]

where $\rho_{\text{Al}_2\text{O}_3}$ and $\rho_{\text{Fe-Al}}$ denote the density of alumina particles and the bulk metal, respectively, $\Sigma s_A(I)$ and $\Sigma s_A(T)$ represent the area occupied by alumina particles and total investigated area, respectively. M_O and $M_{\text{Al}_2\text{O}_3}$ are the atomic and molecular weights of oxygen and alumina, respectively. In most of the cases, the denominator constitutes the term $\rho_{\text{Fe-Al}}[\Sigma s_A(T)]M_{\text{Al}_2\text{O}_3}$ only, as area occupied by inclusions $\Sigma s_A(I)$ is much smaller compared to the total observed area $\Sigma s_A(T)$ and hence its contribution can be ignored.

III. RESULTS

A. Aluminum Oxygen Data Using ICP-AES and LECO

The compositional data obtained for aluminum (using ICP-AES) and oxygen (dissolved and total) measured using two-stage combustion analysis are summarized in Table II. Two-stage heating method in an inert gas fusion infrared absorption method leads to the development of a technique which enables the simultaneous analysis of O and TO in steel samples.[20] This study was limited to an ultra-low carbon, Al-killed steels with other elements/impurities present in traces. The aluminum concentration in the study was analogous to a typical deoxidation range (0.0285–0.0380 wt pct). The insoluble oxygen was reported as 5.3 ± 5.1 for an Al concentration of 0.0285 wt pct, while as it was 8.1 ± 2.5 ppm for the Al concentration of 0.038 wt pct. The present work has been mainly focused on the steel containing high Al concentration.

From Table II, it can be seen that, in the low Al content range, the concentration of dissolved oxygen (O) drops sharply from the initial oxygen content of around 0.0119 wt pct to about 0.0010 wt pct as the Al content increases from 0.0735 to 0.14 wt pct. The O content remains within a very narrow range of 0.0002 to 0.0006 wt pct (2 to 6 ppm) in the medium Al concentration range of 0.256 to 3.65 wt pct. The O content seems to be noticeably increasing in the high Al content range (beyond 5.399 wt pct). The maximum O content reported in the present work is 0.0019 wt pct (TO − 0.0027 wt pct) which corresponds to the Al content of 23.35 wt pct (maximum Al content in the present study). The trend is somewhat similar for the total oxygen content. In the low to medium Al content range (0.0735–3.65 wt pct), the TO content mostly varies between 0.0003 and 0.0009 wt pct with a deviant TO content of 0.0016 at Al content of 0.14 wt pct. The TO content varies between 0.0011 and 0.0016 wt pct for medium to high Al concentration of 5.399–9.518 wt pct. In the very high Al concentration (Al ≥ 5.399 wt pct), the TO content is between 0.0018 and 0.0027 wt pct with

Table II. Equilibrium Concentration of Al and O in Steel Measured After Solidifying the Samples

Experiment No.	Wt Pct Al	Wt Pct Dissolved Oxygen (O) ± 0.0004 pct	Wt Pct Insoluble Oxygen (IO) ± 0.0004 pct	Wt Pct of Total Oxygen TO = (O + IO)
1	0.0008	0.0119	0	0.0119
2	0.0091	0.0035	0.000289	0.003789
3	0.0735	0.000909	0.0001	0.000909
4	0.14	0.00107	0.000588	0.001658
5	0.256	0.000642	0.000210	0.000852
6	0.279	0.000441	0.000203	0.000644
7	0.519	0.000225	0.000312	0.000537
8	0.584	0.000303	0.0000303	0.0003333
9	1.132	0.000501	0.000199	0.0007
10	1.386	0.000416	0.000368	0.000784
11	1.57	0.000208	0.000233	0.000441
12	1.704	0.000292	0.000217	0.000509
13	3.65	0.000697	0.000257	0.000954
14	5.399	0.00139	0.000245	0.001635
15	5.462	0.000994	0.000578	0.001572
16	5.805	0.00075	0.000495	0.001245
17	5.985	0.001	0.00019	0.00119
18	8.375	0.00124	0.000385	0.001625
19	9.518	0.0009995	0.000487	0.0014865
20	11.78	0.00123	0.001061	0.002291
21	13.013	0.00103	0.000771	0.001801
22	15.097	0.000776	0.000259	0.001035
23	21.56	0.00123	0.00154	0.00277
24	23.35	0.00191	0.000814	0.002724

some deviant TO value of 0.0010 wt pct which corresponds to 15.09 wt pct. The evolution of O and TO with increasing Al content is seen in Figure 3. With increase in aluminum content above a certain concentration (where oxygen is minimum), the oxygen again increases as reported by several researchers.[1–16]

B. Scanning Electron Microscopy Analysis

Alumina inclusions have been observed in all the steel samples containing varying concentration of aluminum. A typical alumina inclusion observed in a low aluminum content steel (0.0735 wt pct) having a composition (Al – 47.74 wt pct, O – 52.26 wt pct) measured using SEM-EDS along with its elemental mapping is shown in Figure 4.

Pertaining to the two-stage heating during combustion analysis, SEM-EDS analysis has been carried out for a few samples containing high aluminum concentration before combustion (LECO) analysis (Figure 5(a)), after the first-stage heating (Figure 5(b)) and after two-stage heating (Figure 5(c)).
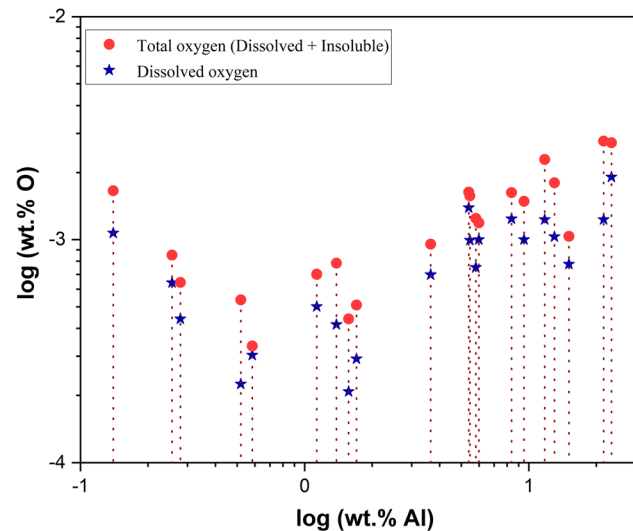
Elemental mapping before the combustion analysis shows a clear alumina inclusion and the dissolved aluminum distributed in the iron matrix. After the first-stage heating at 1873 K, sample was taken out from graphite crucible for SEM analysis. The alumina inclusions were clearly identified (Figure 5(b)) which revealed that alumina was not reduced at 1873 K. Elemental mapping for oxygen reveals a little or no oxygen in the matrix indicating that dissolved oxygen has been mostly removed in single-stage heating. From Figure 4, it is evident that the region surrounding alumina inclusion is devoid of both aluminum and oxygen as the concentration of aluminum in the steel sample is very low. However, the neighborhood of alumina inclusion, in a steel sample containing higher aluminum concentration, clearly shows dissolved aluminum and a little bit of dissolved oxygen (Figure 5(b)). The presence of oxygen in the high aluminum containing iron matrix can be explained by considering the high affinity of dissolved oxygen toward aluminum as compared to the iron. It may also be interpreted that as the aluminum concentration in iron matrix increases, the solubility of aluminum associates and/or oxides increases in iron.

SEM analysis of the steel sample (Al- 23.35 wt pct) taken at different stages of two-stage combustion analysis manifested that insoluble oxygen or oxygen combined with alumina inclusions is released (Figure 5(c)) between temperature range of 1873–2613 K, that is, during the second stage of heating.

C. Scanning Electron Microscopy Automated Inclusion Analysis (SEM-AIA) of Samples

Seven different samples were observed under SEM-AIA for measuring the area fraction of inclusions. As discussed already in the experimental section, Eq. [4] was used to calculate the amount of insoluble oxygen quantitatively. A comparative analysis between insoluble oxygen determined using SEM-AIA and LECO (two-stage heating method) is given in Table III and shown in Figure 6.

D. Thermodynamic Analysis

Thermodynamic analysis for Fe-Al-O system has been carried out using three different formalisms, namely, (i) Wagner's interaction parameter formalism (WIPF) truncated at the 2nd order, (ii) Darken's quadratic formalism, and (iii) the Cubic formalism

Fig. 3—Relationship between total (dissolved + insoluble) and dissolved oxygen with aluminum concentration (wt pct Al > 0.1).
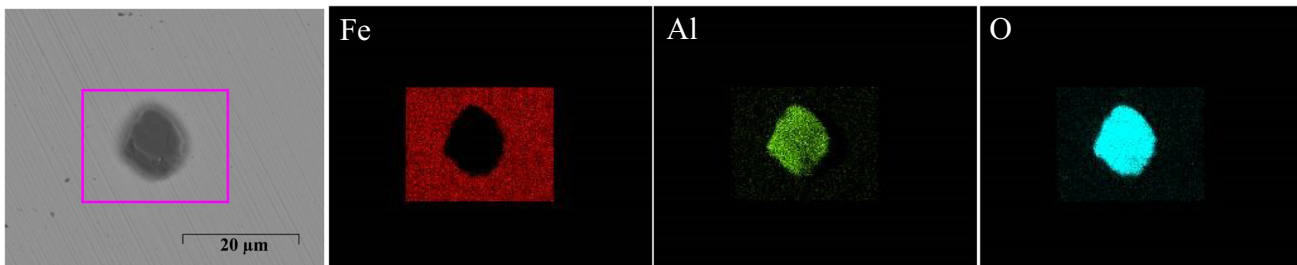

Fig. 4—Alumina inclusion in a steel sample (Al- 0.0735 wt pct) along with its elemental mapping.
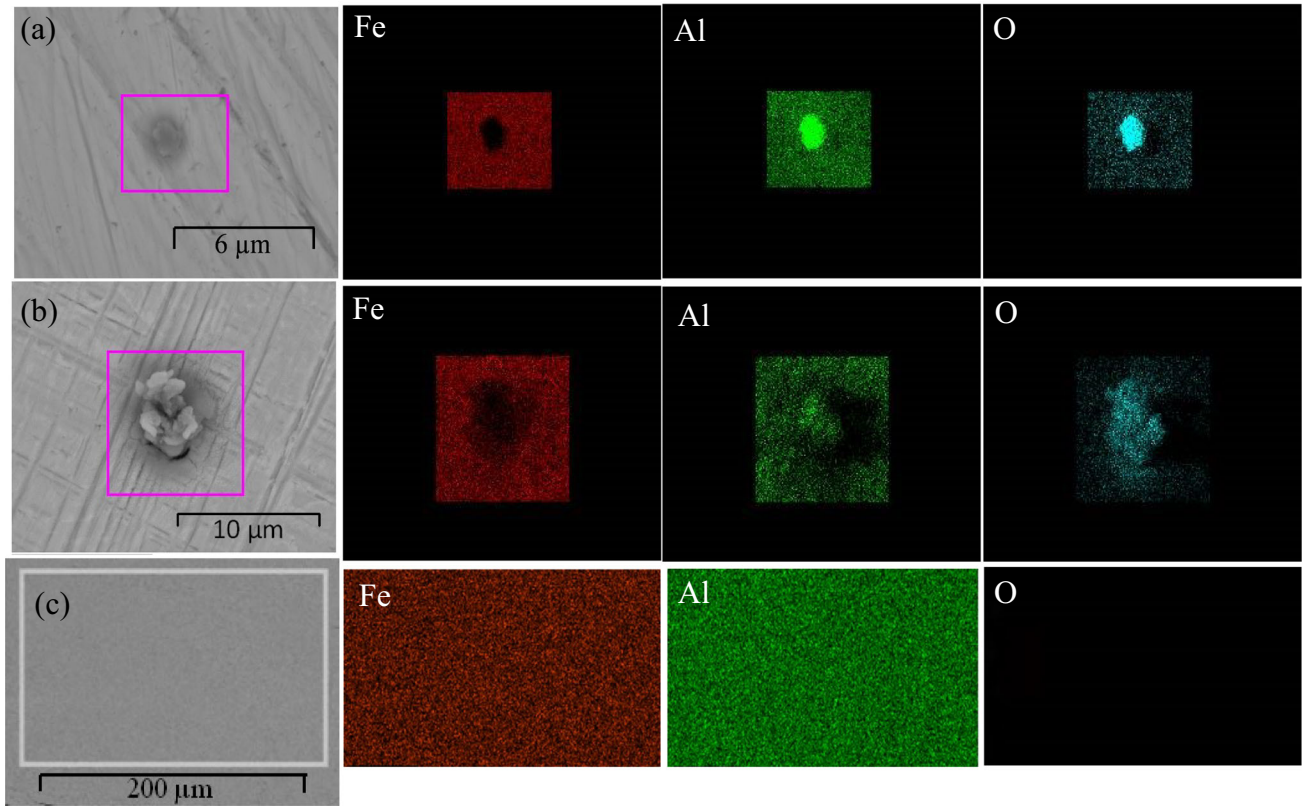
Fig. 5—Elemental mapping of the steel sample (Al- 23.35 wt pct) in LECO at various stages (*a*) before two-stage heating (*b*) after the 1st stage heating and (*c*) after the 2nd stage heating.

**Table III. Insoluble Oxygen Obtained by Using SEM-AIA and Two-Stage Heating (LECO) Analysis**

Aluminum (Wt Pct)	Measured Area in SEM-AIA (mm^2)	Inclusion Area (μm^2)	Insoluble Oxygen Calculated Using SEM-AIA in Wt Pct	Insoluble Oxygen Measured Using LECO in Wt Pct Accuracy $\pm$ 0.0004 Pct
3.65	9.2233	73.122	0.000191	0.000257
5.462	5.6729	40.454	0.000174	0.000578
8.375	7.1956	81.7044	0.000285	0.000385
9.518	13.4415	310.7876	0.000587	0.000487
13.013	11.6966	51.677	0.0001157	0.000771
15.097	9.4824	95.1988	0.0002677	0.000259
23.35	3.0435	182.067	0.0017083	0.000814

1. *Wagner's Interaction Parameter Formalism (WIPF)*

Wagner interaction parameter formalism (WIPF)[21] is a popular formalism to describe the activity coefficient of solute elements present in a very dilute solution. The activity coefficient is represented by an infinite Taylor series. The detailed description can be found in our previous manuscript.[31]

In Fe-Al-O ternary system of regular Al-killed steels, aluminum concentration and the corresponding equilibrium oxygen content are very small as compared to the Fe concentration. WIPF can provide a good approximation of the equilibrium constant and the other thermodynamic parameters for such a Fe-Al-O system.

The deoxidation reaction can be written as

$$2\underline{Al} + 3\underline{O} = (Al_2O_3)_{solid} \qquad [5]$$
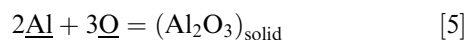
The equilibrium constant K_1 for Eq. [5] is given as

$$K_1 = \frac{a_{Al_2O_3}}{(h_{Al})^2(h_O)^3}, \qquad [6]$$

where h_i denotes activity of component 'i' on a 1 wt pct standard state

$h_{Al} = f_{Al}(\text{wt pct Al}), \quad h_O = f_O(\text{wt pct O})$ and, $a_{Al_2O_3} = 1$ (considering it as pure)

where f_{Al} and f_O denote the activity coefficients of solutes aluminum and oxygen on a 1 wt pct scale, respectively.

$$2\log(f_{Al}) + 2\log(\text{wt pct Al}) + 3\log(f_O)$$
$$+ 3\log(\text{wt pct O})$$
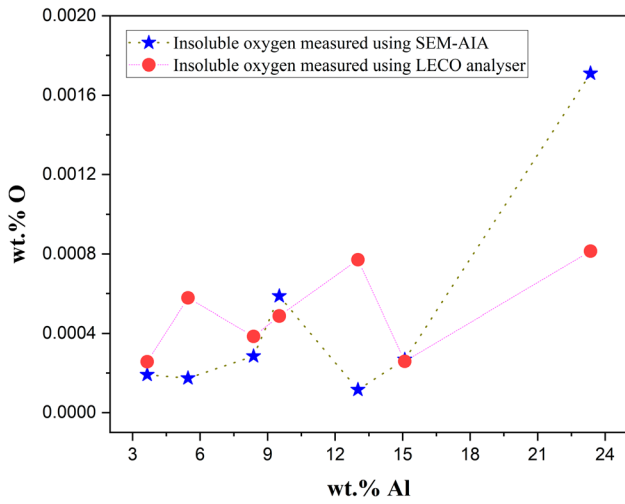$$= \log\frac{1}{K_1} \qquad [7]$$

Fig. 6—Comparison of insoluble oxygen determined using two-stage heating (LECO) and SEM-AIA analysis.
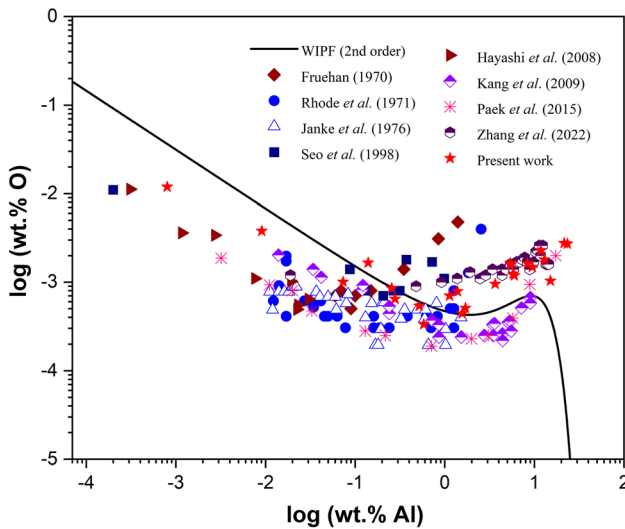

Fig. 7—Al–O (wt pct) equilibria in liquid iron considering total oxygen (TO) at 1873 K. Symbols denote the experimental data and the solid line represents the curve obtained by using WIPF (truncated at the 2nd order).

Using the interaction parameters up to the second order (ignoring the 3rd and higher order ones),

$$
\begin{aligned}
& 2e_{Al}^{Al}(\text{wtpctAl}) + 2e_{Al}^{O}(\text{wtpctO}) + 2r_{Al}^{Al}(\text{wtpctAl})^2 \\
& \quad + 2r_{Al}^{O}(\text{wtpctO})^2 + 2r_{Al}^{Al,O}(\text{wtpctAl})(\text{wtpctO}) \\
& \quad + 2\log(\text{wtpctAl}) + 3e_{O}^{Al}(\text{wtpctAl}) + 3e_{O}^{O}(\text{wtpctO}) \\
& \quad + 3\log(\text{wtpctO}) + 3r_{O}^{O}(\text{wtpctO})^2 + 3r_{O}^{Al}(\text{wtpctAl})^2 \\
& \quad + 3r_{O}^{Al,O}(\text{wtpctAl})(\text{wtpctO}) \\
& = \log K
\end{aligned}
$$

[8]

where $K = (1/K_1)$

For assessing the thermodynamic equilibrium between Al and total oxygen (which is basically the dissolved oxygen at 1873 K, see the discussion section), we have used interaction parameter values (1st and 2nd order at 1873 K)

Using Lupis relationships[32] and substituting values of $e_{Al}^{Al} = 0.043$ [17], $e_{O}^{O} = -0.174$ [17] and $r_{Al}^{Al} = -0.001$[33] $r_{O}^{O} = 0$[33]

$$
\begin{aligned}
& -2\log(\text{wtpctAl}) - 3\log(\text{wtpctO}) - 0.086(\text{wtpctAl}) \\
& \quad + 0.528(\text{wtpctO}) + 0.00431(\text{wtpctAl})(\text{wtpctO}) \\
& \quad + 0.002(\text{wtpctAl})^2 \\
& = e_{O}^{Al}[3(\text{wtpctAl}) + 3.375(\text{wtpctO}) \\
& \quad - 0.06375(\text{wtpctO})(\text{wtpctAl})] + r_{O}^{Al}[3(\text{wtpctAl})^2 \\
& \quad + 6.75(\text{wtpctAl})(\text{wtpctO})] + r_{Al}^{O}[2(\text{wtpctO})^2 \\
& \quad + 3.56(\text{wtpctAl})(\text{wtpctO}] - \log K
\end{aligned}
$$

[9]

Eq. [9] can be represented in the form of Eq. [10] as

$$
y = \lambda_1 x_1 + \lambda_2 x_2 + \lambda_3 x_3 + C
$$

[10]

Using multiple linear regression, the values of different interaction parameters obtained with the R^2 as 0.95 are given below.

$$
e_{O}^{Al} = -0.212 \pm 0.02
$$

$$
r_{O}^{Al} = 0.0089 \pm 0.0014
$$

$$
r_{Al}^{O} = -25.2661 \pm 9.275
$$

and, $\log K = -10.51 \pm 0.1966$

Using the values of these interaction parameters and $\log K$, a relationship between wt pct Al and wt pct total oxygen can be obtained as shown in Figure 7. The experimental data reported by other researchers and the present work have been also included.

Using the experimental data of wt pct Al and wt pct $\underline{O}$ (dissolved oxygen) in Eq. [9], the values of interaction parameters and $\log K$ now will change. Using the multiple linear regression with R^2 of 0.952, the interaction parameters determined are given below.

$$
e_{O}^{Al} = -0.21553 \pm 0.01888
$$

$$
r_{O}^{Al} = 0.008725 \pm 0.001107
$$

$$
r_{Al}^{O} = -37.1791 \pm 12.46
$$

and, $\log K = -11.10683 \pm 0.178$

Using the above interaction parameters in Eq. [9], the relationship between wt pct $\underline{O}$ and wt pct Al can be obtained as shown in Figure 8.
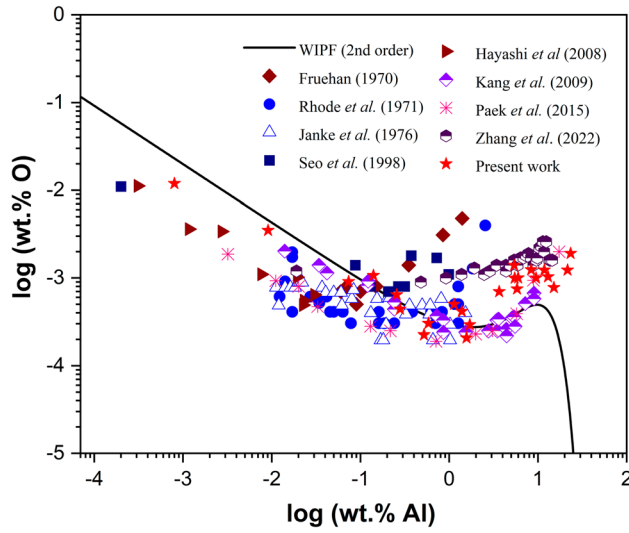
Fig. 8—Al-O (wt pct) equilibria considering soluble/dissolved (O) oxygen in liquid iron at 1873 K. Symbols denote the experimental data and the solid line represents the curve obtained by using WIPF (truncated at the 2nd order).
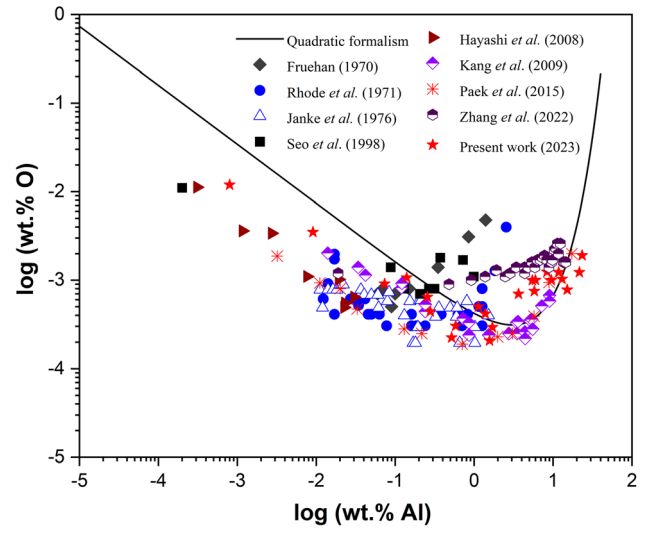

Fig. 10—Al-O (wt pct) equilibria considering soluble/dissolved (O) oxygen in liquid iron at 1873 K. Symbols denote the experimental data and the solid line represents the curve obtained by using Darken's formalism.
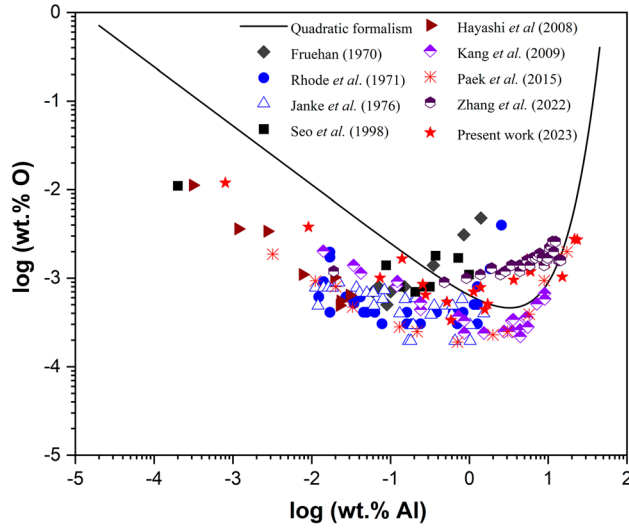

Fig. 9—Al–O (wt pct) equilibria in liquid iron considering total oxygen (TO) at 1873 K. Symbols denote the experimental data and the solid line represents the curve obtained by using Darken's formalism.

2. Darken's Quadratic Formalism

The excess molar free energy g^E can be expressed as the polynomial of degree 2 as mentioned by Darken[22]

$$\frac{g^E}{RT} = x_{Fe}x_{Al}\left[\omega_0^{Fe,Al}\right] + x_{Fe}x_O\left[\omega_0^{Fe,O}\right] + x_{Al}x_O\left[\omega_0^{Al,O}\right] + C_1 x_{Al} + C_2 x_O$$

[11]

$\omega_0^{i,j}$ denote the dimensionless coefficients (i and j can be Fe, Al, O)

Eq. [11] can be written as

$$\frac{g^E}{RT} = \frac{n_{Fe}n_{Al}}{n^2}\left[\omega_0^{Fe,Al}\right] + \frac{n_{Fe}n_O}{n^2}\left[\omega_0^{Fe,O}\right] + \frac{n_{Al}n_O}{n^2}\left[\omega_0^{Al,O}\right] + \frac{n_{Al}}{n}C_1 + \frac{n_{Al}}{n}C_2$$

[12]

$$\ln\gamma_{Al} = \frac{\partial}{\partial n_{Al}}\left\{(n_{Fe} + n_{Al} + n_O)\frac{g^E}{RT}\right\}$$ [13]

and

$$\ln\gamma_O = \frac{\partial}{\partial n_O}\left\{(n_{Fe} + n_{Al} + n_O)\frac{g^E}{RT}\right\}$$ [14]

On substituting Eq. [12] in Eqs. [13] and (14), [15] and [16] can be obtained, respectively,

$$\ln\gamma_{Al} = \omega_0^{Fe,Al} - 2\omega_0^{Fe,Al}(x_{Al})$$
$$- \left(\omega_0^{Fe,Al} + \omega_0^{Fe,O} - \omega_0^{Al,O}\right)x_O + \omega_0^{Fe,Al}(x_{Al})^2$$
$$+ \omega_0^{Fe,O}(x_O)^2 + (\omega_0^{Fe,Al} + \omega_0^{Fe,O} - \omega_0^{Al,O})x_{Al}x_O$$
$$+ C_1$$

[15]

$$\ln\gamma_O = \omega_0^{Fe,O} - 2\omega_0^{Fe,O}(x_O)$$
$$- \left(\omega_0^{Fe,Al} + \omega_0^{Fe,O} - \omega_0^{Al,O}\right)x_{Al} + \omega_0^{Fe,Al}(x_{Al})^2$$
$$+ \omega_0^{Fe,O}(x_O)^2 + (\omega_0^{Fe,Al} + \omega_0^{Fe,O} - \omega_0^{Al,O})x_{Al}x_O$$
$$+ C_2$$

[16]

For aluminum deoxidation reaction given in Eq. [5],

Table IV. Dimensionless coefficients used in Cubic formalism at 1873 K

Parameter	Numerical value	References
$\omega_0^{Fe,Al}$	-4.6095	[15]
$\omega_1^{Fe,Al}$	0.741	[15]
$\omega_0^{Fe,O}$	-9.548	[34]
$\omega_1^{Fe,O}$	4.9872	[34]
$\omega_0^{Al,O}$	-29.0123	Present study

$$K_2 = \frac{a_{Al_2O_3}}{(a_{Al})^2(a_O)^3} \quad [17]$$

where a_i denotes activity of components. $a_{Al} = \gamma_{Al}(x_{Al})$, $a_O = \gamma_O(x_{Al})$ and, $a_{Al_2O_3} = 1$ (Considering it as pure)

$$2\ln\gamma_{Al} + 2\ln x_{Al} + 3\ln\gamma_O + 3\ln x_O = \ln K, \text{ where } K = \frac{1}{K_2}, \quad [18]$$

where γ_{Al} and γ_O denote the activity coefficients of solutes, aluminum and oxygen, respectively.

It should be mentioned here that the numerical values of equilibrium constant (K_1 in Eq. [6] and K_2 in Eq. [17]) differ because of the different standard states considered. In Eqs. [15] and [16], there are three unknowns ($\omega_0^{Fe,Al}$, $\omega_0^{Fe,O}$, and $\omega_0^{Al,O}$), apart from C_1 and C_2. Among these unknowns, the values of $\omega_0^{Fe,Al}$ and $\omega_0^{Fe,O}$ have been taken as -4.6095[15] and -9.548[34], respectively. An analogy between the Darken's quadratic formalism and WIPF (truncated at the 2nd order) along with the special relations obtained among the interaction parameters by applying Gibbs-Duhem Equation (that is, by making WIPF thermodynamically consistent) can be obtained. Thus, the dimensionless coefficients from Darken's quadratic formalism can be made analogous to the interaction parameters from WIPF (truncated at the 2nd order).[21–23,35] Using this analogy, $\omega_0^{Fe,Al} + C_1$ can be written as $\ln\gamma_{Al}^o$ and its value has been taken as -3.8632.[5] Similarly, $\omega_0^{Fe,O} + C_2$ can be written as $\ln\gamma_O^o$ and its value has been taken as -4.568.[34]

Substituting Eqs. [15] and (16) along with the values of dimensionless coefficients taken from the literature[5,15,34] in Eq. [18], Eq. [19] can be obtained.

Eq. [19] is written in the form of $y = mx + c$ for the determination of unknowns, namely, $\omega_0^{Al,O}$ and $\ln K$,

$$21.4304 - 85.603x_O - 60.9105x_{Al} + 23.0475(x_{Al})^2$$
$$+ 47.74(x_O)^2 + 70.7875x_{Al}x_O - 2\ln x_{Al} - 3\ln x_O$$
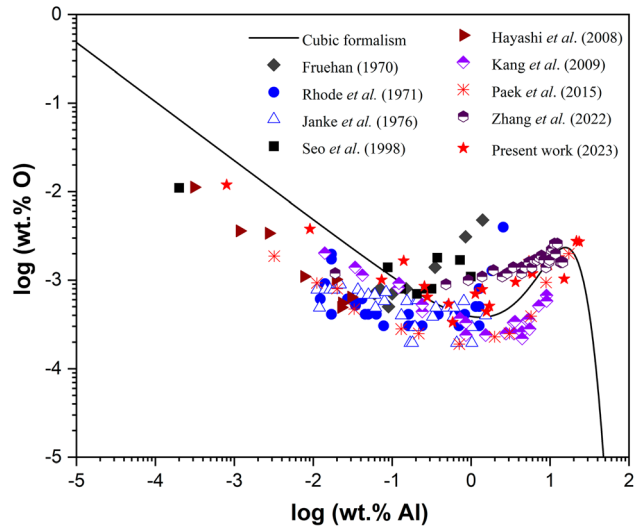$$= (2x_O - 5x_{Al}x_O + 3x_{Al})\omega_0^{Al,O} - \ln K \quad [19]$$

Fig. 11—Al–O (wt pct) equilibria in liquid iron considering total oxygen (TO) at 1873 K. Symbols denote the experimental data and the solid line represents the curve obtained by using Cubic formalism.

Using the experimental data of Al-O equilibria from the present study (wt pct Al and wt pct total oxygen), the values of $\omega_0^{Al,O}$ and $\ln K$ using multiple linear regression (with R^2 value 0.95) are found to be -29.0123 ± 1.47 and -61.90165 ± 0.7, respectively. Substituting the values of $\ln K$ and $\omega_0^{Al,O}$ in Eq. [19], Eq. [20] can be obtained.

$$3\ln x_O = -2\ln x_{Al} - 27.5784x_O - 74.274x_{Al}x_O$$
$$+ 26.1264x_{Al} + 23.0475(x_{Al})^2 + 47.74(x_O)^2$$
$$- 40.47125$$

$$[20]$$

The mole fractions of aluminum and oxygen given in Eq. [20] have been converted to wt pct and obtained the relationship between wt pct O (where O is TO) and wt pct Al as shown in Figure 9. In the subsequent results, similar conversion from mole fraction to wt pct has been done to obtain the relationship between aluminum and oxygen.

The values of $\omega_0^{Al,O}$ and $\ln K$ using multiple linear regression (with R^2 value 0.946) and experimental data for O are found to be -29 ± 1.48 and -63.278 ± 0.686, respectively. The relationship between wt pct Al and wt pct dissolved oxygen has been obtained by substituting these values in Eq. [19] and is shown in Figure 10

3. Assessment of Fe-Al-O Equilibria Using Cubic Formalism

As mentioned by Eleno and Schön,[36] the excess molar free energy of a ternary system can be obtained from Redlich-Kister polynomial of the 3rd order as shown in Eq. [21].

$$\frac{g^E}{RT} = x_{Fe}x_{Al}\left[\omega_0^{Fe,Al} + \omega_1^{Fe,Al}(x_{Fe} - x_{Al})\right]$$
$$+ x_{Fe}x_O\left[\omega_0^{Fe,O} + \omega_1^{Fe,O}(x_{Fe} - x_O)\right]$$
$$+ x_{Al}x_O\left[\omega_0^{Al,O} + \omega_1^{Al,O}(x_{Al} - x_O)\right]$$
$$+ x_{Fe}x_{Al}x_O\omega^{Fe,Al,O} \qquad [21]$$

$\omega_0^{i,j}, \omega_1^{i,j}$ and $\omega^{Fe,Al,O}$ represent the dimensionless coefficients (i and j can be Fe, Al, O)

The expressions for $\ln\gamma_{Al,}$(as shown in Eq. [22]) and $\ln\gamma_O$(as shown in Eq. [23]) can be obtained from Eq. [21] by multiplying it with total number of moles and then partially differentiating with respect to number of moles of aluminum and oxygen, respectively.[23,35]

$$\ln\gamma_{Al} = \omega_0^{Fe,Al} + \omega_1^{Fe,Al} + \left(-2\omega_0^{Fe,Al} - 6\omega_1^{Fe,Al}\right)x_{Al}$$
$$+ \left(-\omega_0^{Fe,Al} - 2\omega_1^{Fe,Al} - \omega_0^{Fe,O} - 2\omega_1^{Fe,O} + \omega_0^{Al,O} + \omega^{Fe,Al,O}\right)x_O$$
$$+ \left(\omega_0^{Fe,Al} + 9\omega_1^{Fe,Al}\right)(x_{Al})^2$$
$$+ \left(\omega_0^{Fe,O} + \omega_1^{Fe,Al} + 6\omega_1^{Fe,O} - \omega_1^{Al,O} - \omega^{Fe,Al,O}\right)(x_O)^2$$
$$+ \left(\omega_0^{Fe,Al} + 8\omega_1^{Fe,Al} + \omega_0^{Fe,O} + 4\omega_1^{Fe,O} - \omega_0^{Al,O}\right.$$
$$\left. + 2\omega_1^{Al,O} - 3\omega^{Fe,Al,O}\right)x_{Al}x_O$$
$$- (4\omega_1^{Fe,Al})(x_{Al})^3 - (4\omega_1^{Fe,O})(x_O)^3$$
$$+ \left(-6\omega_1^{Fe,Al} - 2\omega_1^{Fe,O} - 2\omega_1^{Al,O} + 2\omega^{Fe,Al,O}\right)(x_{Al})^2 x_O$$
$$+ \left(-2\omega_1^{Fe,Al} - 6\omega_1^{Fe,O} + 2\omega_1^{Al,O} + 2\omega^{Fe,Al,O}\right)x_{Al}(x_O)^2 \qquad [22]$$

$$\ln\gamma_O = \omega_0^{Fe,O} + \omega_1^{Fe,O}$$
$$+ \left(-\omega_0^{Fe,Al} - 2\omega_1^{Fe,Al} - \omega_0^{Fe,O} - 2\omega_1^{Fe,O} + \omega_0^{Al,O} + \omega^{Fe,Al,O}\right)x_{Al}$$
$$+ \left(-2\omega_0^{Fe,O} - 6\omega_1^{Fe,O}\right)x_O$$
$$+ \left(\omega_0^{Fe,Al} + 6\omega_1^{Fe,Al} + \omega_1^{Fe,O} + \omega_1^{Al,O} - \omega^{Fe,Al,O}\right)(x_{Al})^2$$
$$+ \left(\omega_0^{Fe,O} + 9\omega_1^{Fe,O}\right)(x_O)^2$$
$$+ \left(\omega_0^{Fe,Al} + 4\omega_1^{Fe,Al} + \omega_0^{Fe,O} + 8\omega_1^{Fe,O}\right.$$
$$\left. - \omega_0^{Al,O} - 2\omega_1^{Al,O} - 3\omega^{Fe,Al,O}\right)x_{Al}x_O$$
$$- (4\omega_1^{Fe,Al})(x_{Al})^3 - (4\omega_1^{Fe,O})(x_O)^3$$
$$+ \left(-6\omega_1^{Fe,Al} - 2\omega_1^{Fe,O} - 2\omega_1^{Al,O} + 2\omega^{Fe,Al,O}\right)(x_{Al})^2 x_O$$
$$+ \left(-2\omega_1^{Fe,Al} - 6\omega_1^{Fe,O} + 2\omega_1^{Al,O} + 2\omega^{Fe,Al,O}\right)x_{Al}(x_O)^2 \qquad [23]$$

The values of dimensionless coefficients are taken from Table IV. An analogy of Eqs. [22] and [23] with Wagner's 3rd order Taylor series[21,23] considering thermodynamic consistency, $\omega_0^{Fe,Al} + \omega_1^{Fe,Al}$ can be written as $\ln\gamma_{Al}^o$ and its value has been taken as -3.8685. Similarly, $\omega_0^{Fe,O} + \omega_1^{Fe,O}$ can be written as $\ln\gamma_O^o$ and its value has been taken as -4.5608. These values have been slightly different from the values used in Darken's quadratic formalism. Using all these values in Eq. [18] and

expressing it in the form of $y = \beta_1 X_1 + \beta_2 X_2 + C$ for determination of $\omega_1^{Al,O}$, $\omega^{Fe,Al,O}$, and $\ln(K)$, Eq. [24] can be obtained.

$$21.4194 + 69.3876x_{Al} + 85.104x_O - 18.5901(x_{Al})^2$$
$$- 148.2428(x_O)^2 - 254.6124x_{Al}x_O + 72.102(x_{Al})^2 x_O$$
$$+ 157.026(x_O)^2 x_{Al} + 14.82(x_{Al})^3 + 99.744(x_O)^3 - 2\ln x_{Al} - 3\ln x_O$$
$$= \left[3(x_{Al})^2 - 2(x_O)^2 - 2x_{Al}x_O - 10(x_{Al})^2 x_O + 10(x_O)^2 x_{Al}\right]\omega_1^{Al,O}$$
$$+ \left[3x_{Al} + 2x_O - 3(x_{Al})^2 - 2(x_O)^2 - 15x_{Al}x_O\right.$$
$$\left. + 10(x_{Al})^2 x_O + 10(x_O)^2 x_{Al}\right]\omega^{Fe,Al,O} - \ln K$$
$$[24]$$

Based on the experimental data of Al-O (TO) and using multiple linear regression (with R^2 value 0.87), the values of $\omega_1^{Al,O}$, $\omega^{Fe,Al,O}$, and $\ln K$ are obtained as $37.1848, -3.8613$, and -64.4443, respectively.

Substituting these values in Eq. [24], Eq. [25] can be obtained. On the conversion of mole fraction to wt pct in Eq. [25], the relationship between wt pct O (total oxygen)) and wt pct Al can be obtained as shown in Figure 11.

$$-43.0249 + 80.9715x_{Al} + 92.8266x_O - 141.7284(x_{Al})^2$$
$$- 81.5958(x_O)^2 - 238.1623x_{Al}x_O + 482.563(x_{Al})^2 x_O$$
$$- 176.209(x_O)^2 x_{Al} + 14.82(x_{Al})^3 + 99.744(x_O)^3$$
$$- 2\ln x_{Al} - 3\ln x_O = 0$$
$$[25]$$

The values of $\omega_1^{Al,O}$, $\omega^{Fe,Al,O}$, and $\ln K$ have been obtained as $37.6691, -3.2947$ and -65.4488, respectively, based on the multiple linear regression (with R^2 value 0.90) of Al-O (O) experimental data. Similarly, substituting these values in Eq. [24], the relationship between wt pct O (dissolved oxygen) and wt pct Al can be obtained as shown in Figure 12.

IV. DISCUSSION

The present work of establishing the Al-O equilibria at 1873 K can be distinguished from the previous studies on the basis of (i) experimental methodology, particularly the oxygen analysis and (ii) the thermodynamic analysis, that is, application of thermodynamically consistent higher order formalisms.

A. *Experimental Analysis*

The melting experiments were carried out by the researchers either in an induction furnace or in a resistance heated furnace. In a resistance heated furnace, a fairly constant temperature zone can be achieved (within a temperature variation of ±2 K) as compared to the induction furnace whereby, because of eddy currents in the melt, the temperature control of melt is arduous. The other problem could be the introduction of oxide particles to the melt through the erosion of
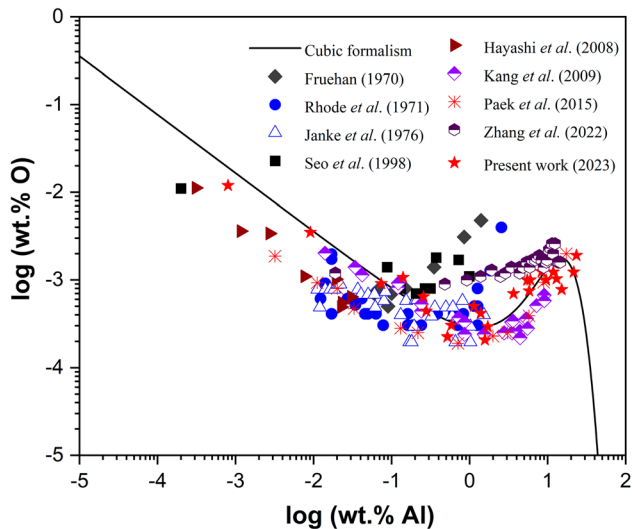
Fig. 12—Al-O (wt pct) equilibria considering soluble/dissolved (O) oxygen in liquid iron at 1873 K. Symbols denote the experimental data and the solid line represents the curve obtained by using Cubic formalism.

$$l = \frac{2}{9\eta} r^2 (\rho_s - \rho_l) g t, \qquad [26]$$

where $l(\text{maximum}) = 1.5$ cm, $\eta = 0.0055 \frac{Ns}{m^2}$, $\rho_s = 3950 \frac{kg}{m^3}$, $\rho_l = 7000 \frac{kg}{m^3}$, $g = 9.8 \frac{m}{s^2}$ and $t = 7200 s$

The sampling was done in the central bottom (CB) portion of the sliced section (shown in Figure 2) from where most of the primary oxides have already been floated to the top portion. The alumina inclusions present in the analyzed samples could mostly be the secondary inclusions. It is possible that some of the primary inclusions with size less than 2.6 μm might also be present in the samples. Therefore, it poses quite an interesting challenge to draw a proper analysis regarding the true equilibrium between aluminum and (O/TO) oxygen at 1873 K. In the present study, we have not been referring dissolved aluminum and total aluminum specifically as both will be almost equal. This is because aluminum is in weight percent and aluminum combined with inclusions is in the ppm level. So, any separate determination of soluble and insoluble aluminum was not required as our analysis was mainly focused on the high aluminum concentration.

Owing to the present sampling methodology, it can be assumed that all the large-sized primary oxides have been floated from the analyzed portion (CB). Therefore, in principle, the total oxygen measured in the solid samples should be same as the dissolved oxygen at 1873 K. For the sake completeness, all the possibilities in connection with the presence of suspended primary oxides and precipitated secondary oxides are summarized in Table V.

The contribution of oxygen present in the form of oxides (also referred as combined oxygen or insoluble oxygen (IO)) has been corroborated by measuring the insoluble oxygen by using two different techniques, namely, LECO (two-stage heating) and SEM-AIA. The SEM-AIA analysis has been done mainly on the samples in the high aluminum concentration range. As can be seen from Figure 6, there is a reasonable agreement between the insoluble oxygen (IO) measured by LECO (two-stage) and the IO estimated based on the area fraction of inclusions obtained with SEM-AIA especially in the medium to high aluminum concentration range. The contribution of this insoluble oxygen ranges between 2 and 5 ppm (0.0002 to 0.0005 wt pct) for an aluminum content up to 15.097 wt pct (Tables II and III). The contribution of insoluble oxygen becomes prominent in the high Al concentration (23.35 wt pct) and accounts for 17 ppm (SEM-AIA) and 8.14 ppm (LECO), respectively. Therefore, there was indeed secondary precipitation of alumina, homogenously (fresh nucleation of alumina) and/or heterogeneously (growth of suspended primary alumina inclusions) during cooling.

The insoluble oxygen present in the samples originates from the suspended primary oxides having size less than 2.6 μm (type I) + homogenously precipitated secondary oxides (type II) + the growth of suspended primary inclusions due to secondary precipitation on it (type (I + II)). It can be expected that majority of the oxide

crucible wall because of continuous stirring due to electromagnetic forces. In the present study, the resistance heated furnace (Carbolite GERO) has been used. Furthermore, an individual experiment has been carried out for every concentration of aluminum and the corresponding equilibrium oxygen, thus ensuring the same initial conditions for all the experiments. With the fixed initial conditions, the continuous addition of deoxidizer (aluminum) and subsequent sampling at regular intervals of time have been completely eliminated. The contribution of oxygen from the primary oxides has been minimized in the present experiments as sufficient time (2 h) for the equilibration and the flotation of alumina particles was provided. Moreover, the sampling location (central bottom region of the solidified ingot) was defined for all the experiments.

Fast cooling of the steel sample taken from the melt is a crucial factor. Irrespective of the cooling rate (fast/slow) from liquidus to solidus temperature, the secondary precipitation of alumina inclusions is inevitable. The actual dissolved oxygen can only be determined when the steel is in molten state at 1873 K. In the present work, since equilibration time of melt at 1873 K was 2 h, it can be expected that the most of the primary oxides would float as per Stokes law (Eq. [26]) assuming negligible natural convection in the melt. The alumina particles with size greater than 2.6 μm present near the bottom of the crucible can traverse a distance of 1.5 cm, while the inclusions with size greater than 1.5 μm present/formed in the center of sliced section (meant for characterization) would be floated away from the central bottom region.

Table V. Summary of Various Scenarios Corresponding to the Presence of Primary and Secondary Oxides

Possibilities/scenarios				
Contribution of oxides				
	Primary	Secondary	Interpretation	Conclusion
I	high/significant	high/significant	TO $\neq$ $\underline{O}$ at 1873 K and it would be difficult to estimate the true $\underline{O}$ and true TO at 1873 K by analyzing solid samples	this scenario is ruled out since the individual values of insoluble oxygen measured in the solid samples (for most experiments) are not very high so the contribution of both (primary and secondary) cannot be high.
II	high/significant	low/insignificant	TO $\neq$ $\underline{O}$ at 1873 K, however, $\underline{O}$ at 1873 K will approximately correspond to $\underline{O}$ measured in the solid samples.	$\underline{O}$ measured in the solid samples would provide an estimate for $\underline{O}$ present at 1873 K
III	low/insignificant	high/significant	TO~$\underline{O}$ at 1873 K and $\underline{O}$ present at 1873 K is approximately equal to TO in the solid samples.	TO measured in the solid samples would provide an estimate for $\underline{O}$ present at 1873 K
IV	low/insignificant	low/insignificant	TO~$\underline{O}$ at 1873 K and $\underline{O}$ present at 1873 K is approximately equal to TO/$\underline{O}$ in the solid samples.	TO/$\underline{O}$ measured in the solid samples would provide an estimate for TO/$\underline{O}$ present at 1873 K. However, this scenario can also be ruled out since the difference between TO and $\underline{O}$ is not nil/insignificant. (especially in the high Al concentration range)

particles present in the samples were of type (I + II) as the growth of existing primary oxides (type I) due to secondary precipitation would be energetically favorable under furnace cooling as compared to the nucleation of fresh secondary oxides (type II).

Considering the above possibilities, it is difficult to quantify the oxygen present purely as primary or purely as secondary alumina inclusions. Therefore, one possibility is that the total oxygen measured in the solidified samples is same as the dissolved oxygen present at 1873 K, assuming the contribution of insoluble oxygen, essentially coming from the suspended alumina particles, was very small (Al-TO equilibria). This corresponds to the scenario III in Table V. The other possibility (which corresponds to scenario II in Table V) is that the contribution of insoluble oxygen due to the suspended primary oxides has been substantial and the contribution of heterogeneously precipitated secondary oxides was extremely small as the time for solidification was rather limited (15 to 20 mins). In that case, the measured dissolved oxygen in the solidified samples can only be termed as the true $\underline{O}$ (Al-$\underline{O}$ equilibria). Both these possibilities are schematically represented in Figure 13. Based on these arguments and interpretation/conclusions in Table V, it is not difficult to fathom that the actual equilibrium oxygen content has to be somewhere between the measured $\underline{O}$ and TO in the solid samples ruling out the two extremes, that is, scenario I and IV in Table V. The difference between the TO and $\underline{O}$ seems to be neither too significant nor completely insignificant indicating that the contribution of insoluble oxygen (devoid of its origin primary/secondary) is quantifiable under the present experimental conditions. So, the Al-O (where O can be $\underline{O}$ or TO)

equilibria have been established separately. The shifting of equilibrium with continuous cooling cannot be asserted as there was no holding time for a particular time interval until the sample solidifies. Recently, it has been shown in the study carried out for Si-O equilibria at 1873 K in liquid iron[37] where a similar cooling rate was followed. The total oxygen content measured in the Fe-Si-O melt equilibrated at 1873 K for 2 h followed by furnace cooling was higher than the total oxygen content measured in the samples which, after equilibrating at 1873 K for 2 h were held at 1823 K for another 1 h followed by furnace cooling. This substantiates the fact that equilibrium would shift, if sufficient time is provided for the equilibration and the flotation of oxide particles.

In the result section (see Table II and Figures 7 through12), it has been observed that with the addition of aluminum, the concentration of oxygen decreases initially. In the present study, the minimum dissolved oxygen content has been measured as 2.08 ppm at aluminum concentration of 1.57 wt pct. The maximum dissolved oxygen at high aluminum concentration was measured to be 19.1 ppm for a corresponding equilibrium Al concentration of 23.35 wt pct. The minimum total oxygen of 3.33 ppm and the maximum total oxygen of 27.24 ppm have been reported in the present study. A comparison of the experimental results recently obtained/reported by Zhang et al.[16] shows that the oxygen content obtained in the present study is relatively lower. This could be because of our unique sampling methodology whereby only one sample, from the central bottom portion of the melt, has been obtained from each experiment. The samples were cut from the solidified ingot (central bottom region) (see

Figure 2) to minimize the contribution of non-metallic particles (alumina) in estimating the dissolved oxygen content. In combination with this unique sampling methodology, there could be several reasons for low oxygen content such as (a) any kind of contamination through a sampler was avoided (b) equilibration time was kept 2 h which provided sufficient time for inclusion flotation and thereby, the contribution of oxygen through primary alumina particles in our samples has been minimized (iii) liquid metal cooled inside the furnace preventing its exposure to the atmosphere. All of these factors have prevented overestimation in the analysis of oxygen. Furthermore, the separate analysis of dissolved and insoluble oxygen made a clear distinction between the oxygen content which often reported as the same in the previous studies.

B. Thermodynamic Analysis

As discussed in the previous section, the distinction between the total oxygen and dissolved oxygen is not obvious. Therefore, thermodynamic assessment in the present study has been carried out for both, total (TO) and the dissolved oxygen (O) using all the three
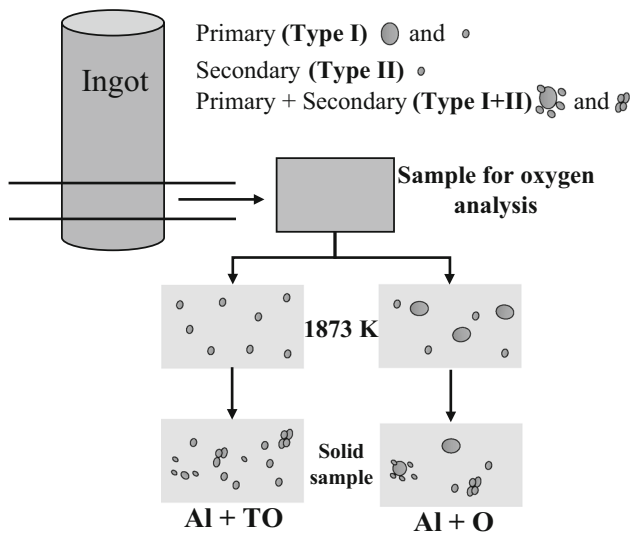

Fig. 13—Schematic representation of primary and secondary inclusions present in the steel samples. Al-TO and Al-O correspond to scenario III and II, respectively, in Table V.

formalisms, namely (A) Wagner's interaction parameter formalism (WIPF) truncated at the 2nd order (also known as Lupis Elliott's formalism), (B) Darken's quadratic formalism, and (C) the Cubic formalism. Since the study was focused on the high Al steels, the formalisms having at least second or higher order terms have been employed. The latter two formalisms (B) and (C) are thermodynamically consistent, while the WIPF (truncated at 2nd order) is thermodynamically inconsistent. The values of interaction parameters and the equilibrium constant estimated using WIPF truncated at the 2nd order did not differ much for the TO and O as can be seen in Table VI. The value of $\log K$ calculated with the present experimental data using this formalism (WIPF truncated at the 2nd order) is larger than the values reported by other researchers listed in Table I except with that of Hilty et al.[1] and Zhang et al.[16] The value of e_O^{Al} (Table VII) obtained is less negative (larger) as compared to the values obtained by all the researchers listed in Table I. The relatively less negative values of e_O^{Al} have also been obtained by Kang et al.[13] and Zhang et al.[16] It should be noted here that Kang et al.[13] conducted experiments using master alloy of Fe-Al rather than direct deoxidation with Al similar to the present work. With such experimental method, that is, by equilibrating the pre-melted alloy of Fe-Al with liquid iron, the inclusions were often observed to be minimized in the melt.

WIPF (truncated at the 1st order) only exhibits a local minimum. The incorporation of the second-order interaction parameters into the WIPF (truncated at the 2nd order) results in a local maximum, in addition to a local minimum. In the previous study[31] using WIPF (truncated at 2nd order), the relationship between wt pct O and wt pct Al had been obtained based on the Al-O equilibrium data reported by several researchers. The first-order interaction parameters, and the equilibrium constant was taken from JSPS[17], while the second-order interaction parameters were employed from the compilation.[33] However, the value of r_O^{Al} was taken as zero in that study which resulted in the omission of variable (wt pct O)^2 in the calculations. Only a few researchers reported the values of the second-order cross-interaction parameters. The reported values of second-order cross-interaction parameters such as r_O^{Al} and r_{Al}^O by Paek et al.[15] vary in the range of −500 to 500 and −16000 to 5000 , respectively. In the present work,

Table VI.   Value of $\log K$, Interaction Parameters on wt pct Scale $\left(e_j^{(i)}, r_j^{(i)}, r_k^{(i,j)}\right)$ and on Mole Fraction Scale $\left(\in_j^{(i)}, \rho_j^{(i)}, \rho_k^{(i,j)}\right)$

Interaction Parameters Using WIPF Truncated at 2nd Order (1873 K)	
Al and Total Oxygen (TO)	Al and Dissolved Oxygen (O)
$\log K = -10.51$	$\log K = -11.10683$
$e_O^{Al} = -0.212, e_{Al}^{(O)} = -0.361$	$e_O^{Al} = -0.21553, e_{Al}^{(O)} = -0.37$
$r_O^{Al} = 0.0089, r_{Al}^O = -25.2661$	$r_O^{Al} = 0.008725, r_{Al}^O = -37.1791$
$r_{Al}^{(Al,O)} = 0.034, r_O^{(Al,O)} = -29.94$	$r_{Al}^{(Al,O)} = 0.0337, r_O^{(Al,O)} = -44.064$
$\in_{Al}^{(Al)} = 5.3, \ \in_O^{(Al)} = \in_{Al}^{(O)} = -23.056, \ \in_O^{(O)} = -10.75$	$\in_{Al}^{(Al)} = 5.3, \ \in_O^{(Al)} = \in_{Al}^{(O)} = -23.45, \ \in_O^{(O)} = -10.75$
$\rho_O^{(Al)} = 35.545, \rho_{Al}^{(O)} = -47710.27, \rho_{Al}^{(Al,O)} = 99.95, \rho_O^{(Al,O)} = -95408.23$	$\rho_O^{(Al)} = 34.654, \rho_{Al}^{(O)} = -70198.26, \rho_{Al}^{(Al,O)} = 98.058, \rho_O^{(Al,O)} = -140383.83$

using the regression analysis, the value of r_O^{Al} has been estimated as -37.8309 for $\underline{O}$ (-25.2661 for TO) based on experimental analysis of the Al-O equilibria. It has been observed that the nature of the curve is dependent mostly on the coefficients of wt pct Al, (wt pctAl)^2 and predominantly on $\log K$. The values of other interaction parameters can be found using Lupis relationships.[32]

WIPF (truncated at 2nd order) is thermodynamically inconsistent and devoid of any constraints, that is, there is no direct relationship between the 1st and 2nd order interaction parameters. The thermodynamic consistency in WIPF (truncated at 2nd order) can be brought in by obtaining special relationships between the interaction parameters by applying Gibbs-Duhem equation.[23] Such thermodynamically consistent WIPF (truncated at 2nd order) imposes a constraint by establishing a direct relationship (also termed as the Lupis relationship) between the 1st and the 2nd order interaction parameters. Darken's quadratic formalism and unified interaction parameter formalism (UIPF) (truncated at 1st order) are analogous to this thermodynamically consistent WIPF (truncated at 2nd order).

Darken's quadratic formalism for assessing thermodynamic equilibria has been explained separately[23] which yielded a direct relationship between the 1st and 2nd order interaction parameters considering its analogy with WIPF (truncated at 2nd order). For example, as per Darken's formalism (Table VIII), the value of $\in_{Al}^{(O)}$

Table VII. Values of log *K* and e_O^{Al} Obtained by Various Researchers

Researcher	Value of log *K*	Value of e_O^{Al}
Hilty and Crafts[1]	−8.53	—
Gokcen and Chipman[2]	−13.68	−12
Mclean and Bell[3]	−13.9	−4.6
Fruehan [5]	−13.35	−3.9
Rhode *et al.*[6]	−13.57	−1.17
Janke and Fischer[7]	−13.62	−1
Dimitrov *et al.*[10]	−14.01	−5.54
Kang *et al.*[13]	−11.52	−0.23
Zhang *et al.*[16]	−10.18	−0.286
Present study	−10.51 (for TO), −11.07 (for $\underline{O}$)	−0.212 (for TO), −0.216 (for $\underline{O}$)

or $\in_O^{(Al)}$ is equal to $-\left(\omega_0^{Fe,Al} + \omega_0^{Fe,O} - \omega_0^{Al,O}\right)$ and comes out to be – 14.855 for TO (– 14.843 for $\underline{O}$). The magnitude of this cross-interaction parameter $\left(\in_{Al}^{(O)}\right.$ or $\left.\in_O^{(Al)}\right)$ comes out to be smaller than the one obtained in WIPF (2nd order) formalism. The other interaction parameters obtained using this formalism are also given in Table VIII.

WIPF truncated at the 2nd order with thermodynamic consistency violates the Lupis relationship and all the 2nd order interaction parameters can be obtained from the 1st order interaction parameters. However, there is no relationship between the 1st order and 2nd order interaction parameters compiled by Sigworth and Elliott[33] estimated on the basis of experimental data. Therefore, higher order formalisms (beyond the 2nd order) should be developed despite the fact that lower order formalisms (such as 1st and 2nd order) are mathematically simple, require less interaction parameters, and can be made thermodynamically consistent. The development of higher order formalisms such as Cubic and Quartic have outlined in the authors' previous work.[23] For cubic order, the values of interaction parameters and their analogous dimensionless coefficients ($\omega_k^{i,j}$ and $\omega^{i,j,k}$) are tabulated in Table IX. These parameters have been obtained by comparing expressions for $\ln \gamma_{Al}$ and $\ln \gamma_O$ from Eqs. [22] and [23] with Wagner's truncated Taylor series as discussed in our previous article.[23] From Table IX, it can be seen that the 3rd order interaction parameters are reported for the first time in the present study.

The relationship obtained between wt pct Al and wt pct O (TO and $\underline{O}$) using three formalisms can be compared with the present experimental data as shown in Figure 14. A comparison of interaction parameters in WIPF (truncated at 2nd order), Darken's formalism, and Cubic formalism given in Tables VI, VIII, and IX clearly indicates that there is a little difference for the two sets of aluminum-oxygen data, that is, between Al and $\underline{O}$ and Al and TO. The first-order cross-interaction parameters obtained by using all the three formalisms are negative and are responsible for attaining a minimum in the Al-O equilibria. The second-order cross-interaction and ternary interaction parameters are positive and negative for WIPF (2nd order) and Cubic formalism. The positive values of these second-order

Table VIII. Interaction Parameters and Dimensionless Coefficients Estimated Using Darken's Formalism

Interaction Parameters Using Darken's Quadratic Formalism (1873 K)

Al and Total Oxygen (TO)	Al and Dissolved Oxygen ($\underline{O}$)
$\in_{Al}^{(Al)} = -2\omega_0^{Fe,Al} = 9.219$	$\in_{Al}^{(Al)} = -2\omega_0^{Fe,Al} = 9.219$
$\in_O^{(O)} = -2\omega_0^{Fe,O} = 19.096$	$\in_O^{(O)} = -2\omega_0^{Fe,O} = 19.096$
$\rho_{Al}^{(Al)} = \rho_O^{(Al)} = -\frac{\in_{Al}^{(Al)}}{2} = -4.6095$	$\rho_{Al}^{(Al)} = \rho_O^{(Al)} = -\frac{\in_{Al}^{(Al)}}{2} = -4.6095$
$\rho_O^O = \rho_{Al}^{(O)} = -\frac{\in_O^{(O)}}{2} = -9.548$	$\rho_O^O = \rho_{Al}^{(O)} = -\frac{\in_O^{(O)}}{2} = -9.548$
$\rho_{Al}^{(Al,O)} = \rho_O^{(Al,O)} = -\in_O^{(O)} = -\in_O^{(Al)} = \omega_0^{Fe,Al} + \omega_0^{Fe,O} - \omega_0^{Al,O} = 14.855$	$\rho_{Al}^{(Al,O)} = \rho_O^{(Al,O)} = -\in_O^{(O)} = -\in_O^{(Al)} = \omega_0^{Fe,Al} + \omega_0^{Fe,O} - \omega_0^{Al,O} = 14.843$

Table IX. Interaction Parameters/Dimensionless Coefficients Obtained Using Cubic Formalism (1873 K)

Interaction Parameter	Equivalence in Terms of Dimensionless Coefficients	Al and TO	Al and $\underline{O}$
$\in_{Al}^{(Al)}$	$-2\omega_0^{Fe,Al} - 6\omega_1^{Fe,Al}$	4.773	4.773
$\in_O^{(Al)}$ or $\in_{Al}^{(O)}$	$-\omega_0^{Fe,Al} - 2\omega_1^{Fe,Al} - \omega_0^{Fe,O} - 2\omega_1^{Fe,O} + \omega_0^{Al,O} + \omega^{Fe,Al,O}$	-30.173	-29.606
$\in_O^{(O)}$	$-2\omega_0^{Fe,O} - 6\omega_1^{Fe,O}$	-10.827	-10.827
$\rho_{Al}^{(Al)}$	$\omega_0^{Fe,Al} + 9\omega_1^{Fe,Al}$	2.06	2.06
$\rho_O^{(Al)}$	$\omega_0^{Fe,Al} + 6\omega_1^{Fe,Al} + \omega_1^{Fe,O} + \omega^{Al,O} - \omega^{Fe,Al,O}$	45.87	45.787
$\rho_{Al}^{(O)}$	$\omega_0^{Fe,O} + \omega_1^{Fe,Al} + 6\omega_1^{Fe,O} - \omega_1^{Al,O} - \omega^{Fe,Al,O}$	-12.207	-13.258
$\rho_O^{(O)}$	$\omega_0^{Fe,O} + 9\omega_1^{Fe,O}$	35.337	35.337
$\rho_{Al}^{(Al,O)}$	$\omega_0^{Fe,Al} + 8\omega_1^{Fe,Al} + \omega_0^{Fe,O} + 4\omega_1^{Fe,O} - \omega_0^{Al,O} + 2\omega_1^{Al,O} - 3\omega^{Fe,Al,O}$	126.685	125.954
$\rho_O^{(Al,O)}$	$\omega_0^{Fe,Al} + 4\omega_1^{Fe,Al} + \omega_0^{Fe,O} + 8\omega_1^{Fe,O} - \omega_0^{Al,O} - 2\omega_1^{Al,O} - 3\omega^{Fe,Al,O}$	-5.07	-7.738
$\theta_{Al}^{(Al)} = \theta_O^{(Al)}$	$-4\omega_1^{Fe,Al}$	-2.964	-2.964
$\theta_{Al}^{(O)} = \theta_O^{(O)}$	$-4\omega_1^{Fe,O}$	-19.949	-19.949
$\theta_{Al}^{(Al,Al,O)} = \theta_O^{(Al,Al,O)}$	$-6\omega_1^{Fe,Al} - 2\omega_1^{Fe,O} - 2\omega_1^{Al,O} + 2\omega^{Fe,Al,O}$	-96.513	-96.348
$\theta_{Al}^{(Al,O,O)} = \theta_O^{(Al,O,O)}$	$-2\omega_1^{Fe,Al} - 6\omega_1^{Fe,O} + 2\omega_1^{Al,O} + 2\omega^{Fe,Al,O}$	35.242	37.3437

interaction parameters counteract the negative values of the first-order parameters. Therefore, incorporation of these second-order interaction parameters in these formalisms brings a maximum at a certain high aluminum concentration. The variation in the 2nd order interaction parameters estimated using WIPF (truncated at 2nd order) shows relatively less variation as compared to the previous studies.[13,14] The absence of maxima in the Al-O equilibria in case of Darken's formalism can be attributed to the negative values of both, the first- and second-order interaction parameters. This would be evident from Figure 15, where numerical values of the cross-interaction parameters are shown for the three formalisms. In Darken's formalism, as already explained, a direct relationship between the 1st and 2nd order interaction parameter exists thus limiting its utility in thermodynamic assessment of a ternary system. Such formalism violates Lupis Relationship[32] and do not match well with the experimental data compiled by Sigworth and Elliott.[33] In Darken's formalism, the 2nd order interaction parameter ρ_O^{Al} is equal to half of $-\varepsilon_{Al}^{Al}$. Since value of ε_{Al}^{Al} is a positive non-integer, the 2nd order interaction parameter ρ_O^{Al} is also negative. Therefore, Darken's formalism cannot exhibit maxima in the curve rather it tends to make the curve steeper in upward direction after minima.

This necessitates the employment of higher order formalisms like Cubic formalism in the high aluminum concentration range. The relationship between aluminum and oxygen for Cubic formalism showed a similar trend as that obtained by WIPF (2nd order). A comparison between both the curves clearly indicates that the agreement between the thermodynamic analysis

and the experimental data is better with Cubic formalism (Figure 14). The values of each interaction parameter and dimensionless coefficient would change for every (high) order formalism, provided a new set of parameters/coefficients is determined using the regression analysis. For instance, with this approach, the available 1st order interaction parameters/dimensionless coefficients cannot be used for the second-order formalism. However, this leads to increase in the number of unknowns at each (higher) order truncation. In Darken's formalism, only three unknowns need to be determined which is simple to evaluate. In Cubic formalism, eighteen interaction parameters which reduce to seven parameters on using interrelationships need to be determined. For each order of truncation, the interaction parameters are dependent on dimensionless coefficients. The values of these dimensionless coefficients (unknowns) can be substituted in Eqs. [11] and [21] to get excess molar free energy values at a particular equilibrium concentration of solutes.

In our present work, we have taken a few dimensionless coefficients used (determined) in Darken's formalisms and incorporated them in the Cubic formalism. It is preferable to determine all the unknowns for a nth order formalism using sufficient experimental data since it adjusts the values of interaction parameters/dimensionless coefficients providing a better fit with the data. Cubic and Darken's formalism are thermodynamically consistent. However, unlike Darken's formalism, (i) there is no ambiguity in the Lupis relationship and (ii) no direct (one-to-one) relationship between the 1st and 2nd order interaction parameters, in Cubic formalism. The 3rd order
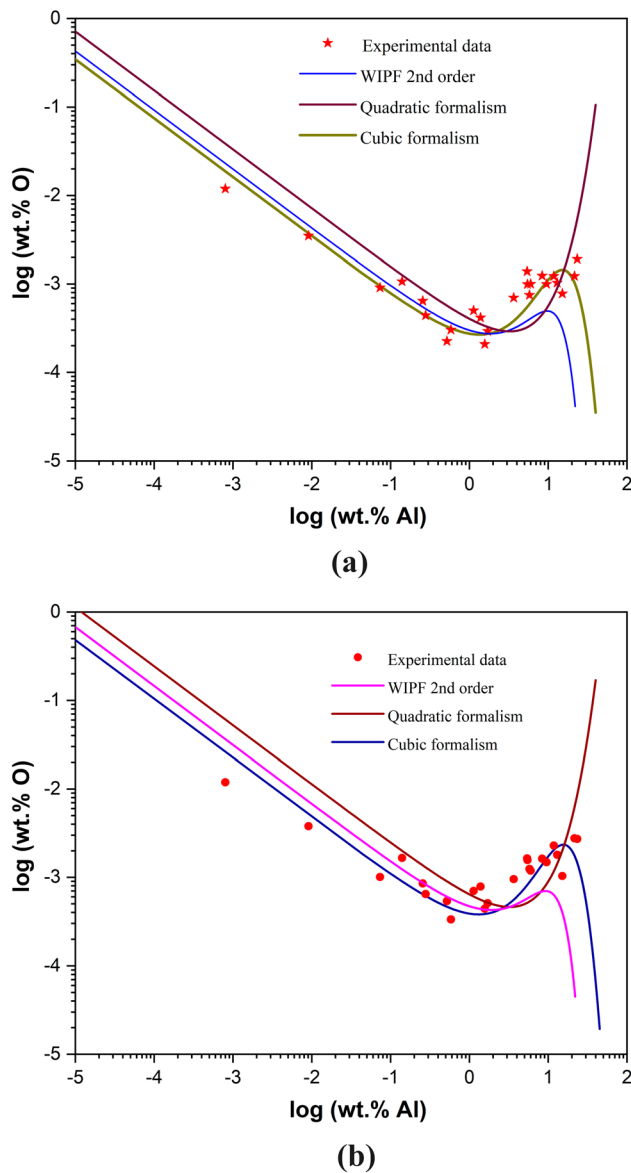
(a)

(b)

Fig. 14—Al-O equilibria using three different formalisms based on (*a*) experimental data consisting of wt pct Al and dissolved oxygen (O) (*b*) experimental data consisting of wt pct Al and wt pct total oxygen (TO).

interaction parameters can be determined from the lower order ones.[23] The reason for employing higher order formalism would be clear on comparing Figures 7 through 12, respectively. The experimental data reported by the researchers, in the high aluminum concentration range, show a good agreement with the Cubic formalism as compared to WIPF (2nd order). It is further evident from Figure 14 that the present experimental data also show the best fit for Cubic formalism.

C. *Minima and Maxima in Al-O Equilibria*

The main constraint in using WIPF in high aluminum concentration is (i) its thermodynamic inconsistency on truncation and the (ii) the unavailability of (higher order) interaction parameters. Our previous work has

led to the development of higher order interaction parameters in a thermodynamically consistent manner.[23] In Fe-Al-O system, to account for the strong interaction between the solutes, namely, aluminum and oxygen, second or higher order interaction parameters are required. The appearance of a minimum and a maximum on the Al-O curve in WIPF (2nd order) and Cubic formalism can be seen in the present work. The minima in the deoxidation curve depend on the type of deoxidizer used. Usually, divalent metals (deoxidizers like Ca, Mg, and Ba) do not exhibit minima in the deoxidation curve.[38] However, dissolved aluminum can react with the deoxidation product, alumina and form associates like Al*O and Al$_2$*O. The oxygen linked with these two associates constitutes a part of dissolved oxygen. If the formation of associates exhibits a significantly negative Gibbs energy of formation, a minimum in deoxidation curve will be observed for the deoxidizer.[38] Modified quasichemical model (MQM) was developed for the assessment of Al-O equilibria in steels by Paek *et al.*[39] MQM considers the strong interaction between Al and O through short-range order. Using MQM, Paek *et al.*[9] extended it for the whole concentration range from 0.0027 to 100 wt pct Al. It must be noted that MQM does not explicitly define a solvent and solute separately. This model showed a minimum at 0.00015 wt pct O corresponding to an aluminum concentration of 0.62 wt pct.[39,40]

The explanation for a minimum in Al-O curve is straightforward and can be attributed to the negative value of the first-order cross-interaction parameter. The negative value accounts for strong interaction between aluminum and oxygen in the low aluminum concentration range. Experimentally, this can be attributed to the lowering of oxygen with increase in aluminum content. As the aluminum concentration increases, the negative value of the first-order cross-interaction parameters can be countered by introducing the second-order interaction parameters which are positive and make the Al-O curve less steep in the medium to high aluminum concentration range. At a reasonably high aluminum concentration, a maximum appears on the Al-O curve. Experimentally, such a maximum on Al-O has not been verified. Only a few researchers have worked in the entire aluminum concentration range and they have not explicitly reported an occurrence of a maximum in their experimental study.[8,14] Shevtsov *et al.*[8] did mention about the second minima in the high aluminum concentration range which was attributed to the formation of (a metastable phase) alumina spinel (Al$_3$O$_4$). Experimentally, Paek *et al.*[14] attempted to determine the oxygen solubility in pure aluminum at 1873 K and admitted that the measured oxygen content was highly scattered. The uncertainty in the oxygen measurement was more than 100 ppm at 1873 K which seems to be the same as reported value of oxygen solubility in pure aluminum melt at 1873 K. They attributed the uncertainty to the suspended alumina particles in pure aluminum melt and overcome this uncertainty using CaO-Al$_2$O$_3$ layer on the top. In Fe-Al-O ternary system, considering extremely low solubility of oxygen in aluminum, it seems unlikely that the maximum

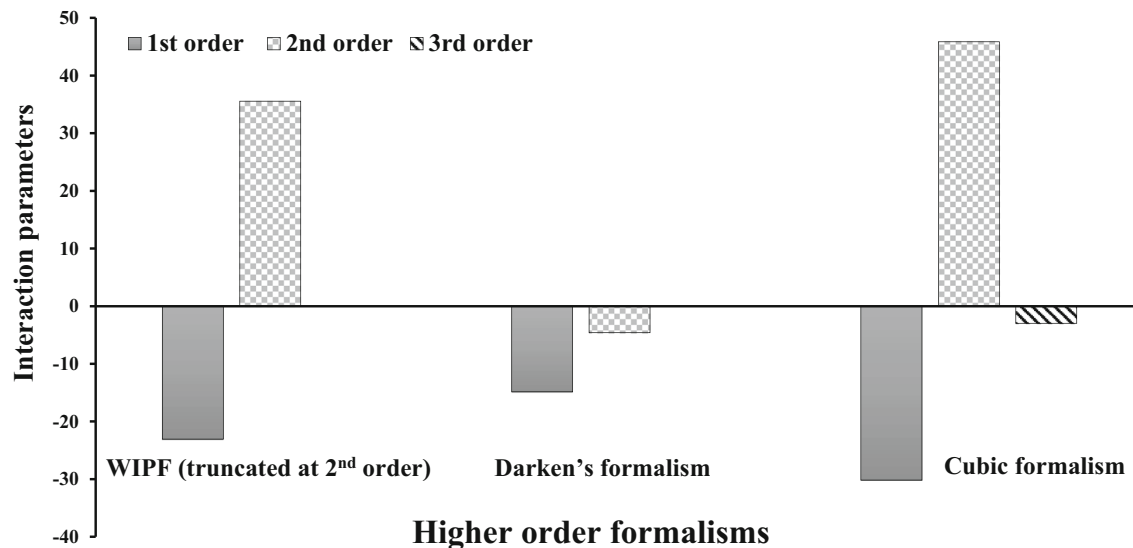Fig. 15—Cross-interaction parameters (Al on O) estimated in the present study ($\epsilon_O^{(Al)}$, $\rho_O^{(Al)}$, and $\theta_O^{(Al)}$).

solubility of oxygen can be found in pure aluminum as compared to Fe-Al alloys. As already mentioned, the increase in the $\underline{O}$ content can be attributed to the tendency of aluminum to retain oxygen in the liquid iron or the presence of Al*O and Al$_2$*O associates in the liquid iron. As the aluminum concentration increases, eventually the precipitation of alumina (or other aluminum oxide) shall occur since the corresponding equilibrium oxygen content would also increase in liquid iron. This precipitation of aluminum oxide in the high aluminum content range may be attributed to the maximum in Al-O curve. Beyond this aluminum concentration, $\underline{O}$ should decrease again in the liquid Fe-Al alloy (as the aluminum concentration approaches 100 pct purity). However, this possibility could not be verified experimentally in the present work since the sample preparation and determination of oxygen became extremely challenging beyond 25 wt pct aluminum in liquid iron. In the thermodynamic analysis, the local maximum has been predicted by using (i) the thermodynamically inconsistent, WIPF (truncated at the 2nd order) and (ii) the thermodynamically consistent, Cubic formalism. However, based on the present work/analysis, the local maximum remains a mathematical artifact (which depends on the values of interaction parameters), lacking empirical substantiation.

V. CONCLUSIONS

The present study was primarily focused on establishing Al-O equilibria at 1873 K in the high aluminum concentration range. The improvement in aluminum-oxygen equilibria has been achieved (i) experimentally by distinguishing $\underline{O}$ from the TO and (2) thermodynamically by using interaction parameter formalisms through development and application of higher order interaction parameter formalism, namely Cubic formalism.

1. Establishing Al-O equilibria at 1873 K has often been a complex task due to the difficulties involved in measuring the dissolved oxygen content at 1873 K by analyzing the solid samples. The oxygen present in the samples has been distinguished for its insoluble content using two different techniques/methodologies, namely, two-stage heating (LECO) and SEM-AIA. There is a reasonable agreement between the insoluble content measured/estimated by these techniques.

2. In the present work, Al-O equilibria have been established for aluminum-dissolved oxygen (Al-$\underline{O}$) and aluminum-total oxygen (Al-TO) using all the three formalisms which include thermodynamically inconsistent, WIPF (2nd order) and thermodynamically consistent, Darken's and Cubic formalisms. The difference between the interaction parameters estimated for Al-$\underline{O}$ and Al-TO was minimal for each of the three formalisms.

3. Based on the WIPF (2nd order), Darken and Cubic formalisms, the thermodynamic data such as the first, second, and third order, cross as well as ternary interaction parameters together with equilibrium constant and dimensionless coefficients (as appropriate) have been estimated using the present experimental data (Al-$\underline{O}$ and Al-TO) and compiled in the present manuscript.

4. The agreement between the experimental data and the thermodynamic analysis has been found to be better with Cubic formalism in the high aluminum concentration range. A thermodynamically consistent, Cubic formalism, predicts maxima in the aluminum-oxygen curve which could not be verified experimentally.

ACKNOWLEDGMENTS

CONFLICT OF INTEREST

No potential conflict of interest was reported by the author(s).

REFERENCES

1. D.C. Hilty and W. Crafts: *Trans. Metall. Soc AIME*, 1950, vol. 188, pp. 181–204.
2. N.A. Gokcen and J. Chipman: *Trans. Metall. Soc. AIME.*, 1953, vol. 194, pp. 173–78.
3. A. McLean and H.B. Bell: *J. Iron Steel Inst.*, 1965, vol. 203, pp. 123–30.
4. J.H. Swisher: *Trans. Metall. Soc. AIME*, 1967, vol. 239, pp. 123–24.
5. R.J. Fruehan: *Metall. Trans.*, 1970, vol. 1, pp. 3403–10.
6. L.E. Rohde, A. Choudhury, and M. Wahlster: *Arch. Eisenhüttenwes.*, 1971, vol. 42, pp. 165–74.
7. D. Janke and W.A. Fischer: *Arch. Eisenhüttenwes.*, 1976, vol. 47, pp. 195–98.
8. V.E. Shevtsov: *Russ. Metall.*, 1981, vol. 1, pp. 52–57.
9. H. Suito, H. Inoue, and R. Inoue: *ISIJ Int.*, 1991, vol. 31, pp. 1381–88.
10. S. Dimitrov, A. Weyl, and D. Janke: *Steel Res.*, 1995, vol. 66, pp. 3–7.
11. J.-D. Seo, S.-H. Kim, and K.-R. Lee: *Steel Res.*, 1998, vol. 69, pp. 49–53.
12. A. Hayashi, T. Uenishi, H. Kandori, T. Miki, and M. Hino: *ISIJ Int.*, 2008, vol. 48, pp. 1533–41.
13. Y. Kang, M. Thunman, D. Sichen, T. Morohoshi, K. Mizukami, and K. Morita: *ISIJ Int.*, 2009, vol. 49, pp. 1483–89.
14. M.-K. Paek, J.-M. Jang, Y.-B. Kang, and J.-J. Pak: *Metall. Mater. Trans. B*, 2015, vol. 46B, pp. 1826–36.
15. H. Fukaya, K. Kajikawa, A. Malfliet, B. Blanpain, and M. Guo: *Metall. Mater. Trans. B*, 2018, vol. 49B, pp. 2389–99.
16. J. Zhang, L. Han, and B. Yan: *Metall. Mater. Trans. B*, 2022, vol. 53B, pp. 2512–22.
17. The 19th Committee in Steelmaking: Thermodynamic Data for Steelmaking, The Japan Society for Promotion of Science (JSPS), Tohoku University Press, Sendai, Japan, pp. 10–13 (2010).
18. H. Yin: *Proc. Int. Conf. AISTech*, 2005, vol. 2, pp. 89–97.
19. Y.-B. Kang, Y.-M. Cho, and H.-M. Hong: *Metall. Mater. Trans. B*, 2022, vol. 53B, pp. 1980–88.
20. H.-M. Hong and Y.-B. Kang: *ISIJ Int.*, 2021, vol. 61, pp. 2464–73.
21. C. Wagner: *Thermodynamics of Alloys*, Addison-Wesley, Reading, 1962, p. 51.
22. L.S. Darken: *Trans. Metall. Soc. AIME*, 1967, vol. 239, pp. 90–96.
23. M. Ishfaq and M.M. Pande: *Steel Res.*, 2023, https://doi.org/10.1002/srin.202200913.
24. A.D. Pelton and C.W. Bale: *Metall. Trans. A*, 1986, vol. 17A, pp. 1211–15.
25. S. Srikanth and K.T. Jacob: *Metall. Trans. B*, 1988, vol. 19B, pp. 269–75.
26. A.D. Pelton: *Metall. Mater. Trans. BMater. Trans. B*, 1997, vol. 28B, pp. 869–76.
27. D.V. Malakhov: *Calphad*, 2013, vol. 41, pp. 16–19.
28. Y.-B. Kang: *Metall. Mater. Trans. B*, 2020, vol. 51B, pp. 795–804.
29. T. Ise, Y. Nuri, Y. Kato, T. Ohishi, and H. Matsunaga: *ISIJ Int.*, 1998, vol. 38, pp. 1362–68.
30. R.T. DeHoff and F.N. Rhines: *Quantitative Microscopy*, McGraw-Hill Publishing Co. Ltd., New York, 1968.
31. M. Ishfaq and M.M. Pande: *Ironmaking Steel Making*, 2022, vol. 50, pp. 44–54.
32. C.H.P. Lupis: *Chemical Thermodynamics of Materials*, North Holland, New York, 1983.
33. G.K. Sigworth and J.F. Elliott: *Metal Science*, 1974, vol. 8, pp. 298–310.
34. T. Miki and M. Hino: *ISIJ Int.*, 2005, vol. 45, pp. 1848–55.
35. C.W. Bale and A.D. Pelton: *Metall. Trans. A*, 1990, vol. 21A, pp. 1997–2002.
36. L.T.F. Eleno and C.G. Schön: *Braz. J. Phys.*, 2014, vol. 44, pp. 208–14.
37. S. Pindar and M.M. Pande: *Steel Res.*, 2023, https://doi.org/10.1002/srin.202300115.
38. I.-H. Jung, S.A. Decterov, and A.D. Pelton: *Metall. Mater. Trans. B*, 2004, vol. 35B, pp. 493–507.
39. M.-K. Paek, J.-J. Pak, and Y.-B. Kang: *Metall. Mater. Trans. B*, 2015, vol. 46B, pp. 2224–33.
40. Y.-B. Kang: *Metall. Mater. Trans. B*, 2019, vol. 50B, pp. 2942–58.